Title

A diverse member of the fungal Avr4 effector family interacts with de-esterified pectin in plant cell walls to disrupt their integrity

Journal

Science Advances, 7(19)

ISSN

2375-2548

Authors

Chen, Li-Hung

Kračun, Stjepan K

Nissen, Karen S

et al.

Publication Date

2021-05-07

DOI

10.1126/sciadv.abe0809

PLANT SCIENCES

A diverse member of the fungal Avr4 effector family interacts with de-esterified pectin in plant cell walls to disrupt their integrity

Li-Hung Chen[1,4], Stjepan K. Kračun[2†], Karen S. Nissen[2], Jozef Mravec[2], Bodil Jørgensen[2], John Labavitch[3‡], Ioannis Stergiopoulos[1]*

Effectors are small, secreted proteins that promote pathogen virulence. Although key to microbial infections, unlocking the intrinsic function of effectors remains a challenge. We have previously shown that members of the fungal Avr4 effector family use a carbohydrate-binding module of family 14 (CBM14) to bind chitin in fungal cell walls and protect them from host chitinases during infection. Here, we show that gene duplication in the Avr4 family produced an Avr4-2 paralog with a previously unknown effector function. Specifically, we functionally characterize *Pf*Avr4-2, a paralog of *Pf*Avr4 in the tomato pathogen *Pseudocercospora fuligena*, and show that although it contains a CBM14 domain, it does not bind chitin or protect fungi against chitinases. Instead, *Pf*Avr4-2 interacts with highly de-esterified pectin in the plant's middle lamellae or primary cell walls and interferes with Ca^{2+}-mediated cross-linking at cell-cell junction zones, thus loosening the plant cell wall structure and synergizing the activity of pathogen secreted endo-polygalacturonases.

INTRODUCTION

Plant immunity generally consists of passive and inducible immune responses (*1*). The plant cell wall has a major part in passive defenses, both due to its function as a structural barrier to infections and because changes in its physicochemical composition affect plant development and immunity (*2*, *3*).

Plant cell walls are mainly composed of a dynamic and intricate matrix of cellulose and hemicellulose microfibrils embedded in pectins, a family of complex polysaccharides consisting primarily of homogalacturonan and rhamnogalacturonans (*4*). Homogalacturonan is a linear homopolymer of α-1,4–linked D-galacturonic acid units (GalA) that is deposited in plant cell walls in a highly methyl-esterified form but is subsequently de-esterified by wall-based pectin methylesterases (PMEs) that remove methyl-ester groups (*5*). De-esterified homogalacturonan can then be readily cross-linked by Ca^{2+}, leading to the formation of Ca^{2+} pectate gels known as "egg boxes" that promote cell-cell adhesion (*6*) and further affect the rheology, stiffening, porosity, and permeability of the plant cell wall to enzymes (*7*). Egg-box formation is particularly evident in the middle lamella, the thin pectin layer deposited at the interface between the primary cell walls of adjacent plant cells that bonds them together and prevents loosening of the plant tissue (*8*). Thus, the pattern and degree of esterification of homogalacturonan have profound effects on the cell wall properties and, consequently, on plant tissue plasticity and susceptibility to microbial attacks (*2*, *3*, *7*, *9*).

Owing to its key role in defense and development, plants have developed elaborate mechanisms to regulate the methyl-esterification status of homogalacturonan during growth (*2*, *3*, *7*, *9*). Conversely, microbes also secrete an array of pectic enzymes such as PMEs, pectate lyases, pectin lyases (PNLs), and polygalacturonases (PGs) to degrade de-esterified homogalacturonan and loosen the plant cell wall structure in aid of the infections (*9*). However, the downside of this enzymatic activity is the release from the damaged cell walls of pectic fragments that are perceived by the host as "danger signals," thus activating innate immune responses (*10*). In general, innate immunity in plants is triggered by the perception from cell-surface pattern recognition receptors of danger signals, including broadly conserved microbial components known as "pathogen-associated molecular patterns" and endogenous "damage-associated molecular patterns" (DAMPs) molecules that emanate from cellular damage as a result of microbial activity or trauma (*11*). Oligogalacturonides (OGs), for example, with a degree of polymerization between 10 and 15 (OG10-15) that are released from the hydrolysis of de-esterified homogalacturonan by microbial pectin-degrading enzymes, are well-known elicitors of DAMP-triggered immunity in plants (*12*). Their perception is mediated by the wall-associated kinase 1 receptor and is contingent on their arrangement in an egg-box configuration (*10*, *13*). Notably, a recent study revealed that OGs released from damaged plant cell walls during infections consist of a complex mixture of acetyl- and methyl-esterified OGs that are mainly spurred by pathogen-secreted PNLs (*14*). This contrasts the current model that unesterified OG10-15s derived from the enzymatic activity of PGs are the major DAMPs that accumulate during microbial infections and further highlights the importance of pectin degrading enzymes in plant-microbe interactions.

To suppress or evade innate immunity, in response, pathogens secrete an array of effector proteins that promote parasitic infections. In resistant plants, however, effectors are recognized by cognate resistance proteins, thus eliciting effector-triggered immunity that typically manifests in the hypersensitive response (HR) (*15*). To date, a great deal of effort has been placed on elucidating the function of effectors secreted by plant pathogens (*16*). An example is *Cf*Avr4, an effector from the hemibiotrophic extracellular pathogen of tomato *Cladosporium fulvum*, which uses a family 14 carbohydrate-binding module (CBM14) to bind chitin in fungal cell walls and

[1]Department of Plant Pathology, University of California, Davis, Davis, CA, USA. [2]Department of Plant and Environmental Sciences, University of Copenhagen, Frederiksberg, Denmark. [3]Department of Plant Sciences, University of California, Davis, Davis, CA, USA. [4]Department of Plant Pathology, National Chung Hsing University, Taichung, Taiwan.
*Corresponding author. Email: istergiopoulos@ucdavis.edu
†Present address: Microbial Screening Department, Chr. Hansen A/S, Discovery R&D, Bøge Alle 10-12, Hørsholm DK-2970, Denmark.
‡Deceased.

protect them from chitinases (*17*). Although functional orthologs of *Cf*Avr4 exist in many fungi, microbes generally exhibit diverse effector repertoires that differ even among phylogenetically closely related species (*18*).

Here, we show that gene duplication of Avr4 in the tomato pathogen *Pseudocercospora fuligena* (*19*), a close relative of *C. fulvum* with a similar infection biology, led to the emergence of a candidate effector with a diversified function. Specifically, we show that *Pf*Avr4-2 binds to homogalacturonan with a low degree of esterification in the middle lamella, thus interfering with Ca^{2+}-mediated cross-linking of neighboring homogalacturonan chains and the integrity of the plant cell wall.

RESULTS

*Pf*Avr4-2 is a paralog of *Pf*Avr4

Query of the *P. fuligena* genome (JABCIY000000000) with *Cf*Avr4 revealed the presence of *Pf*Avr4 (*19*) and an additional 101–amino acid–long *Pf*Avr4-2 protein that shares 33% amino acid identity with *Pf*Avr4. *Pf*Avr4-2 (MK410883) consists of a predicted 16-residue N-terminal signal peptide and an 85-residue mature protein that contains a predicted CBM14 chitin-binding domain (Pfam01607) with 10 cysteine (Cys) residues instead of the 8 defining the CBM14 domain of Avr4 proteins (fig. S1A). The *PfAvr4* and *PfAvr4-2* genes are located on different scaffolds of the *P. fuligena* assembly, and no repetitive DNA was identified immediately adjacent to them (fig. S1B), suggesting that they are not embedded within repeat-rich regions of the genome, as is the case with other fungal effectors (*16*). Further examination of the allelic variation present in *PfAvr4-2* in 30 strains of *P. fuligena* collected from Taiwan (n = 1) and Japan (n = 29) indicated the absence of polymorphisms, suggesting the lack of selection pressure from cognate resistance proteins. A blast search against the National Center for Biotechnology Information nr and the Joint Genome Institute MycoCosm databases identified two homologs of *Pf*Avr4-2 in the phylogenetically related species *Pseudocercospora musae* (KXS93729.1; 74.3% identity) and *Pseudocercospora eumasae* (KXS98644.1; 69.3% identity). However, *Pf*Avr4-2 was absent from *Pseudocercospora fijiensis* that, together with *P. eumasae* and *P. musae*, constitute the sigatoka disease complex in banana (*20*). A phylogenetic tree constructed based on an amino acid alignment of the Avr4 and/or Avr4-2 proteins present in *P. fuligena*, *P. musae*, *P. eumusae*, and *C. fulvum* showed that Avr4-2 proteins form a separate orthologous group to the Avr4 ones (fig. S1C), suggesting a gene duplication in an ancestral species that generated two distinct lineages within the Avr4 family. The alignment also showed that amino acids that are critical to chitohexaose [$(GlcNAc)_6$] binding in *Cf*Avr4 (*17*) are not fully conserved in Avr4-2 proteins, suggesting alterations in substrate binding affinity or specificity (fig. S1A).

Further modeling of *Pf*Avr4-2 on the previously determined *Cf*Avr4 and *Pf*Avr4 tertiary structures (*17*, *19*) predicts that the proteins adopt an overall similar architecture of a distorted β-sandwich fold formed by a central β-sheet with three antiparallel β-strands (A1, A2, and A3) and a smaller C-terminal β-sheet with two antiparallel β-strands (B1 and B2). The short N-terminal (H1) and C-terminal (H2) α-helixes as well as the four disulfide bonds that are formed between the eight cysteines present in Avr4 are also predicted to be conserved in *Pf*Avr4-2 (fig. S2, A and B). However, despite these similarities, some notable discrepancies were observed as well. Specifically, the two extra cysteine residues present in *Pf*Avr4-2 are predicted to form an additional disulfide bond (Cys^{57}-Cys^{62}) in the β-turn that is connecting β-strands A2 and A3, and which likely contributes toward stabilizing the turn and constraining the three-dimensional (3D) conformation of the protein. Moreover, the β-turn connecting β-strands B1 and B2 in the C-terminus of Avr4 is predicted to be replaced in *Pf*Avr4-2 by an α-helix (H2). This helix would create an outward bulge that would widen *Pf*Avr4-2's structure at its C-terminus and would further change its electrostatic surface potential by creating a pocket of positive charge that could contribute to the biding of negatively charged molecules (fig. S2, A and B). Notably, the aromatic residues Trp^{100} and Tyr^{103} in *Cf*Avr4 that are critical for $(GlcNAc)_6$ binding are predicted to be replaced in *Pf*Avr4-2 by the positively charged Arg^{84} and the generally unreactive Gly^{87}, respectively, whereas the placement of the small glycine (Gly) and isoleucine (Ile) residues at positions 87 and 88, results in another positively charged residue (Lys^{90}) that is predicted to be protruding toward the substrate (fig. S2C). Overall, the lack of conservation in amino acids that are critical to $(GlcNAc)_6$ binding and the change in the electrostatic surface potential in the C-terminus of Avr4 and *Pf*Avr4-2 suggest that they could be interacting with different substrates.

*Pf*Avr4-2 has functionally diversified from *Pf*Avr4

To search for evidence of substrate diversification, we used an in vitro affinity precipitation assay to test the binding of *Pf*Avr4-2 to chitin and various other insoluble polysaccharides of fungal and plant origin (*19*). Binding specificity was assessed at pH 5.5, pH 7.0, and pH 8.5, as the pH environment may influence the ligand-binding characteristics of carbohydrate-binding modules. At all three pHs, *Pf*Avr4-2 was present only in the unbound fraction, indicating the absence of binding to the chitinous substrates and to the other polysaccharides used in the assay (Fig. 1, A and B). Localization studies on germlings of *Trichoderma viride* (*19*) using *Pf*Avr4 and *Pf*Avr4-2 conjugated to the Alexa Fluor 488 green fluorescent dye further showed that unlike $Pf\text{Avr4}^{488}$, $Pf\text{Avr4-2}^{488}$ does not localize onto fungal cell walls (Fig. 1C). Similar results were obtained when examining the localization of $Pf\text{Avr4}^{RR}$ and $Pf\text{Avr4-2}^{RR}$ conjugated to the red fluorescent dye Rhodamine Red (RR) on mycelia of *P. fuligena* after their treatment with β-1,3-glucans to expose the underlying chitin layer (Fig. 1D). Last, in contrast to *Pf*Avr4, external application of 10 μg of *Pf*Avr4-2 on germlings of *T. viride* failed to protect them from the chitinolytic activity of whole tomato leaf extracts (Fig. 1E) and from bacterial chitinases supplemented with β-1,3-glucanases (Fig. 1F). Together, these results indicate that *Pf*Avr4-2 has functionally diversified from *Pf*Avr4 and other Avr4 family members.

*Pf*Avr4-2 binds to pectin with a low degree of esterification

To explore the carbohydrate-binding specificity of *Pf*Avr4-2, we initially used a carbohydrate microarray spotted with plant and fungal-related polysaccharides, including pectins with various degrees of esterification (fig. S3A). On the basis of the mean intensity of the spots on the microarray, *Pf*Avr4-2 bound primarily to pectins with a low degree of esterification, whereas a negative correlation was observed between the degree of esterification and the intensity of *Pf*Avr4-2 binding. Specifically, binding was observed on lime pectins that were de-esterified either by fungal (F series) and plant (P series) PMEs to a degree of esterification of ≤11 in case of fungal and to a degree of esterification of ≤32 in case of plant PMEs. Binding to

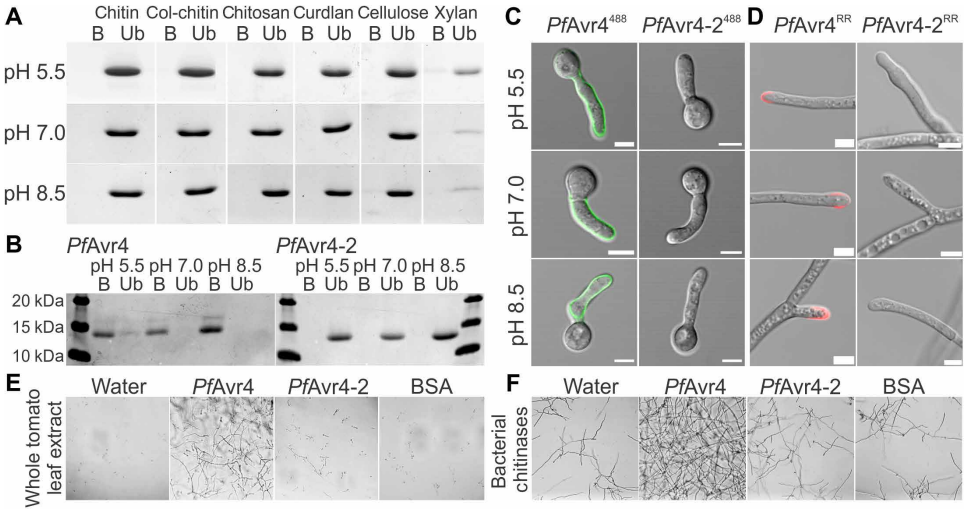

Fig. 1. *Pf*Avr4-2 does not bind chitin or protects fungal hyphae against chitinases. (**A** and **B**) In vitro polysaccharide precipitation assay testing binding of *Pf*Avr4-2 to insoluble polysaccharides of fungal (chitin, colloidal chitin, chitosan, and curdlan) and plant (cellulose and xylan) origin (A) or binding of *Pf*Avr4 (control) and *Pf*Avr4-2 to shrimp shell chitin (B). Binding was tested at pH 5.5, pH 7.0, and pH 8.5. B, bound fraction; Ub, unbound fraction. (**C** and **D**) Localization of *Pf*Avr4 and *Pf*Avr4-2 conjugated to Alexa Fluor 488 (488) or Rhodamine Red (RR) on germlings of *T. viride* (C) and mycelia of *P. fuligena* (D), following their treatment with β-1,3-glucanases to remove the overlaying β-glucan layer in the fungal cell wall. White bars correspond to 5 μm. (**E** and **F**) In vitro assays testing whether *Pf*Avr4 and *Pf*Avr4-2 protect germlings of *T. viride* against plant-derived (E) and bacterial-derived (F) chitinases. Bovine serum albumin (BSA) is used as control.

polygalacturonic acid and sugar-beet pectin with a degree of esterification of 1% was also observed. In contrast, *Pf*Avr4-2 did not interact with other plant or fungal-derived polysaccharides on the array, including short chitin oligosaccharides, β-glucan, xyloglucan, mannan, arabinose, and cellulose (fig. S3A).

To further explore the interaction between *Pf*Avr4-2 and homogalacturonan with a low degree of esterification, we used isothermal titration calorimetry (ITC) to determine the thermodynamic binding parameters between *Pf*Avr4-2 and OG10-15 (fig. S3B). Control titrations of 2 mM OG10-15 mixture into 0.5 mM *Pf*Avr4-2 resulted in a mild heat exchange, indicating weak binding. Although a saturation point could not be reached within a reasonable range of ligand and protein concentrations, the thermodynamic values obtained from fitting a one-site binding model to the isotherm curve showed that *Pf*Avr4-2 bound to the OG10-15 mixture with a dissociation constant (K_d) of 159.9 ± 32.01 μM, a binding enthalpy (ΔH) of −20.48 ± 1.76 kJ/mol, and a stoichiometric ratio (n) of 0.84 ± 0.03. In contrast, control titrations of OG10-15 into the buffer or of the buffer titrated into *Pf*Avr4-2 resulted in no measurable heat change (fig. S3B). Collectively, despite the weak affinity of *Pf*Avr4-2 to OG10-15, the ITC data are suggestive of *Pf*Avr4-2's interaction with galacturonan structures.

*Pf*Avr4-2 interacts with de-esterified pectin in the middle lamella or the primary cell wall

Since pectin is abundantly present in plant cell walls, we examined the localization pattern of *Pf*Avr4-2^{488} on stem cross sections of *Arabidopsis* plants. Labeling was performed at pH 7.0, pH 8.5, and pH 5.5, with the latter reflecting the pH of the tomato apoplast and of the plant cell walls (*21*).

In contrast to *Pf*Avr4^{488}, *Pf*Avr4-2^{488} localized on most stem tissue types, thus corroborating that the two proteins have functionally diversified (Fig. 2A). The localization of *Pf*Avr4-2^{488} on stems was seen only at pH 5.5 (fig. S4A), whereas labeling of the plant stems with *Pf*Avr4-2^{RR} produced the same results, indicating that fluorophore selection did not alter the localization pattern (fig. S4B). *Pf*Avr4-2^{RR} localized in both the dermal and ground tissues of the stem including the epidermis, cortex, and pith parenchyma but only partially in vascular tissue, as the protein bound in the phloem region but not in the xylem (Fig. 2B). Observations at higher magnification showed that *Pf*Avr4-2^{RR} fills the tricellular junctions in the interfascicular fibers (fig. S4C) and in the young pith parenchyma (fig. S4D) but occupies the corners of intercellular spaces at tricellular junctions in the older pith parenchyma toward the stem's center, where cell junctions are expanded and form air-filled intercellular spaces (Fig. 2B and fig. S4D). Staining with the cellulose-binding dye calcofluor white (CW) further showed that *Pf*Avr4-2^{RR} occupies mainly the outer cell wall layers facing the intercellular air spaces, whereas CW binds to the inner cell wall components adjacent to the plasma membrane (Fig. 2B). Similar results were also obtained when examining the localization pattern of *Pf*Avr4-2^{RR} in cross sections of tomato leaves infected with *P. fuligena*, as *Pf*Avr4-2^{RR} was detected proximally to the CW but as a discrete thin layer lining the outer cell wall regions of epidermal cells (Fig. 2C).

The above observations are consistent with *Pf*Avr4-2 localizing at the corners of intercellular spaces at tricellular junctions, the cell wall region facing the intercellular air spaces, and the thin flat sheet lining the outer cell wall regions of neighboring cells, spaces typically occupied by the plant's middle lamella (*8*). Since pectin is the predominant polysaccharide in the middle lamella (*22*), the *Arabidopsis* stem cross sections were treated with commercially available fungal pectinases and were subsequently labeled with *Pf*Avr4-2^{RR}, CW, and JIM7, a monoclonal antibody that specifically recognizes methyl-esterified homogalacturonan (*23*). The pectinase treatment fully abolished the localization of *Pf*Avr4-2^{RR} and JIM7, whereas it had no discernable effect on the labeling intensity and localization pattern of CW (Fig. 2D), thereby suggesting that *Pf*Avr4-2 associates with pectin. Moreover, labeling of *Arabidopsis* stem cross sections

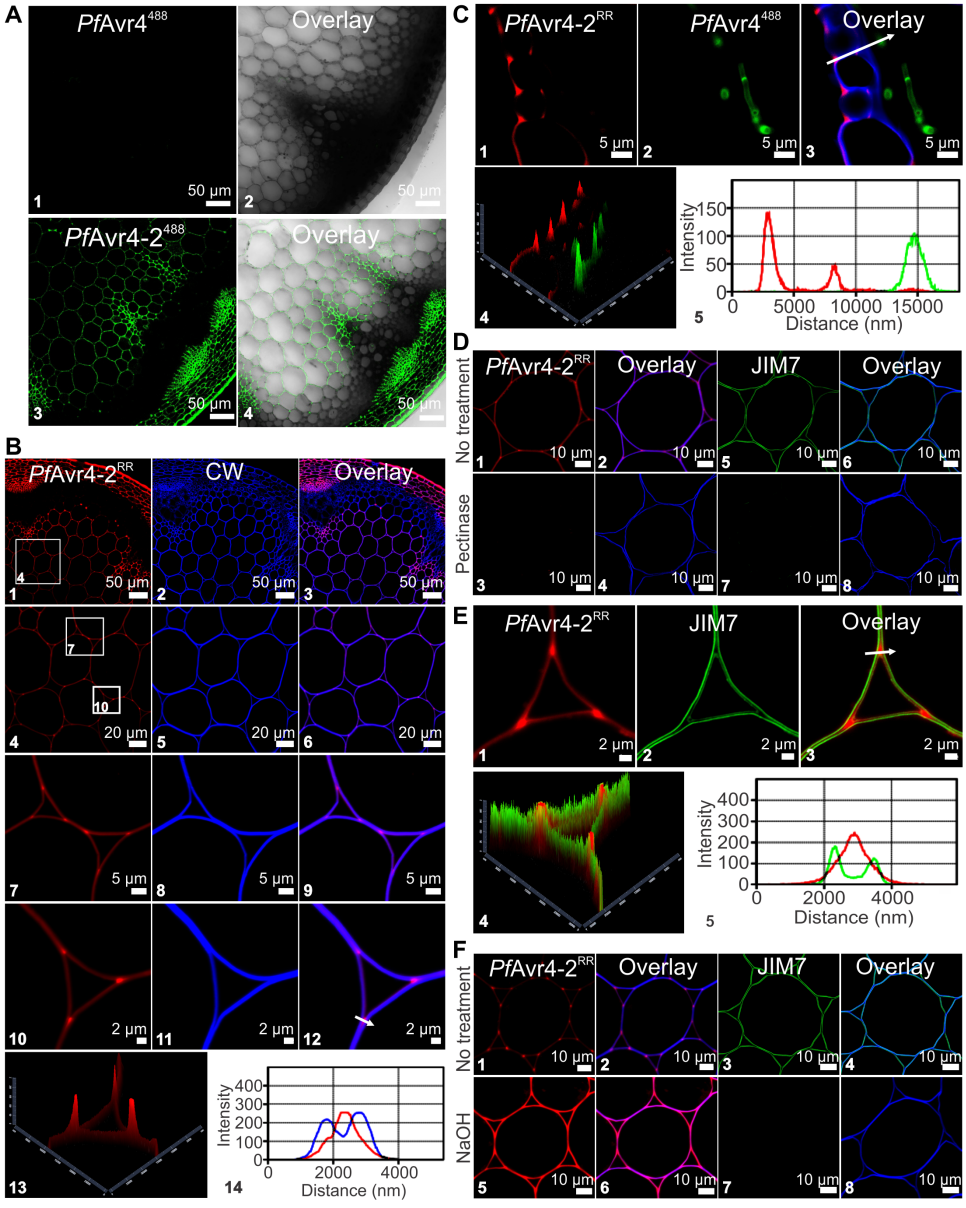

Fig. 2. *Pf*Avr4-2 localizes to pectin-rich regions of the plant cell wall. (**A**) Binding of *Pf*Avr4^{488} and *Pf*Avr4-2^{488} conjugated to Alexa Fluor 488 onto *Arabidopsis* stem cross section; only a quarter of the cross section is shown. (**B**) Dual labeling of *Arabidopsis* stem cross sections with *Pf*Avr4-2^{RR} conjugated to Rhodamine Red (RR) (red signal) and the cellulose-binding protein calcofluor white (CW) (blue signal). White boxes in (B1) and (B4) indicate the sections shown at higher magnification in succeeding panels. Panel (B13) is a 2.5D representation of (B10), whereas the fluorescence intensities of *Pf*Avr4-2^{RR} and CW at the region marked by an arrow in (B12) are shown in (B14). (**C**) Labeling with *Pf*Avr4-2^{RR}, *Pf*Avr4^{488}, and CW of cross sections of tomato leaves infected with *P. fuligena* and sampled at 9 days after inoculation. Panel (C4) is a 2.5D representation of (C3), whereas the fluorescence intensities of *Pf*Avr4-2^{RR} and *Pf*Avr4^{488} at the region marked by an arrow in (C3) are shown in (C5). (**D**) Localization of *Pf*Avr4-2^{RR}, CW, and the JIM7 monoclonal antibody (mAb) on *Arabidopsis* stem cross sections before and after pectinase treatment. A secondary mAb conjugated to Alexa Fluor 488 is used for detecting JIM7. (**E**) Labeling of *Arabidopsis* stem cross sections with *Pf*Avr4-2^{RR} and JIM7. Cells are pith parenchyma and labeling was performed sequentially with the two probes. Panel (E10) is a 2.5D representation of (E9), whereas the fluorescence intensities of *Pf*Avr4-2^{RR} and JIM7 at the region marked by an arrow in (E9) are shown in (E11). (**F**) Labeling of the *Arabidopsis* stem cross sections with *Pf*Avr4-2^{RR}, CW, and JIM7 after pretreatment of the stem with NaOH to chemically de-esterify plant cell walls.

with *Pf*Avr4-2^{RR} and JIM7 showed that the two localize to discrete regions of the cell walls in pith parenchyma cells (Fig. 2E), implying that *Pf*Avr4-2 does not interact with the methyl-esterified homogalacturonan epitope that is recognized by JIM7. Instead, it is plausible that *Pf*Avr4-2 binds pectin in plant cell walls in its fully or highly de-esterified form, as suggested by the carbohydrate microarray data.

To assess this hypothesis, the *Arabidopsis* stem sections were treated with NaOH to induce a random chemical de-esterification of pectin, and labeling was repeated with *Pf*Avr4-2^{RR} and the JIM7 monoclonal antibody. The alkaline pretreatment did not alter their localization pattern on the stem but nearly doubled the labeling intensity of *Pf*Avr4-2^{RR} and almost fully abolished the fluorescence signal of JIM7 (Fig. 2F). This points to a negative correlation

between the degree of esterification of pectin in either the middle lamella or the primary cell wall and its relevance as a binding substrate for *Pf*Avr4-2. This association was further corroborated by examining the localization of *Pf*Avr4-2^{RR} on stem cross sections obtained from two tomato PME-silenced lines (PME RNAi_1 and PME RNAi_2) (*24*). The silencing of PMEs in tomato reduces the de-esterification of homogalacturonan during tissue maturation, thus lowering the amount of potential binding sites. Labeling with *Pf*Avr4-2^{RR} showed that the intensity of the fluorescence signal was nearly abolished (PME RNAi_1) or almost halved (PME RNAi_2) in the stem cross sections of the two PME-silenced lines as compared to the intensity of the fluorescence signal on the wild-type plants (fig. S4, E and F). Furthermore, the difference in fluorescence intensity between the two PME-silenced lines correlated with the silencing levels of PMEs in these plants (*24*). Collectively, these results allude that *Pf*Avr4-2 specifically interacts with homogalacturonan pectin in its highly de-esterified form in either the plant's middle lamella or primary cell wall.

*Pf*Avr4-2 interferes with Ca^{2+}-mediated cross-linking at tricellular junctions

Under native conditions, nonmethylated GalA residues in adjacent homogalacturonan chains can be ionically cross-linked with Ca^{2+} to form egg-box structures that affect the rheological properties of the plant cell wall (*7*). The interaction of *Pf*Avr4-2 with homogalacturonan of low degree of esterification suggests that it is competing with Ca^{2+} for binding to the deprotonated carboxyl groups (COO^-) of nonmethylated GalA residues or, alternatively, that *Pf*Avr4-2 binds to Ca^{2+}-mediated cross-linked homogalacturonan chains. To investigate these hypotheses, we compared the localization pattern of *Pf*Avr4-2^{RR} on *Arabidopsis* stem cross sections with that of the 2F4 monoclonal antibody that specifically binds to Ca^{2+}-mediated cross-linked homogalacturonan (egg boxes) (*13*), and with the OG7-13^{488} probe, a mixture of OG oligomers with a degree of polymerization of 7 to 13 that does not bind to existing egg boxes but forms de novo associations with nonmethylated GalA residues in homogalacturonan chains in the presence of Ca^{2+} (*25*). *Pf*Avr4-2^{RR} and OG7-13^{488} accumulated mostly at the corners and the cell wall region facing the intercellular air spaces at tricellular junctions as well as the thin flat sheet between adjacent cells (Fig. 3A). This suggests the presence in these regions of abundant nonmethylated GalA residues with which the OG7-13^{488} probe can form new egg boxes in the presence of Ca^{2+} ions. The 2F4 monoclonal antibody mainly localized at the cell wall region facing the intercellular air spaces but was less abundant at the corners of tricellular junctions, indicating the limited presence of Ca^{2+}-mediated cross-linked homogalacturonan chains in these regions (Fig. 3B). When a strong Ca^{2+} chelating agent such as EGTA (50 mM) was added to the labeling buffer, the fluorescence intensity of *Pf*Avr4-2^{RR} remained the same, whereas that of the 2F4 monoclonal antibody was nearly abolished, suggesting that the binding of *Pf*Avr4-2 to homogalacturonan with a low degree of esterification does not require Ca^{2+} (Fig. 3C). In contrast, labeling of the *Arabidopsis* stem sections in the presence of increasing calcium concentrations ([Ca^{2+}]) showed that the fluorescence intensities of *Pf*Avr4-2^{RR} and of 2F4 were negatively and positively correlated with [Ca^{2+}] in the labeling buffer, respectively (Fig. 3D). Collectively, the above suggest that *Pf*Avr4-2 competes with Ca^{2+} for binding to free COO^- groups of nonmethylated GalA residues along the homogalacturonan chains.

*Pf*Avr4-2 can partly disrupt egg boxes, thus loosening the cell wall structure

To further assess whether binding of *Pf*Avr4-2 to nonmethylated GalA residues in intermittently Ca^{2+}-mediated cross-linked homogalacturonan chains has any effect on egg boxes, the 2F4 monoclonal antibody and the OG7-13^{488} probe were used to monitor their integrity and formation in the presence of *Pf*Avr4-2. For this purpose, *Arabidopsis* sections were pretreated with *Pf*Avr4-2, and after washing the protein off the tissue, the stem sections were labeled with the OG7-13^{448} probe, the 2F4, or the JIM7 monoclonal antibodies. As controls, the stems were also pretreated with *Pf*Avr4 and wheat germ agglutinin (WGA), as these proteins do not bind pectin or other polysaccharides in plant cell walls.

Labeling with the 2F4 monoclonal antibody of stems pretreated with *Pf*Avr4-2 produced a patchier and less intense fluorescence signal as compared to stems pretreated with *Pf*Avr4 and WGA, whereas the reverse observations were made with the OG7-13^{488} probe (Fig. 4A). This suggest that some of the Ca^{2+}-mediated cross-links in the tricellular junction zones were disrupted by *Pf*Avr4-2, thus generating after its removal more sites for the de novo formation of egg boxes between the OG7-13^{488} probe and nonmethylated GalA residues along the homogalacturonan chains. Moreover, pretreatment with *Pf*Avr4-2 produced no changes in the fluorescence intensity of the JIM7 monoclonal antibody, suggesting that the above observations were not due to *Pf*Avr4-2 modification of the state of pectin methyl-esterification (Fig. 4A).

To further support the notion that *Pf*Avr4-2 might be interfering with Ca^{2+}-mediated cross-linking of homogalacturonan chains, we exposed germinating pollen tubes of tomato to *Pf*Avr4-2^{RR} and examined the effect on pollen tube growth and integrity. Pollen tubes are known for the distinctive spatial distribution of homogalacturonan with a high and low degree of esterification in the tube apex and the tube flanks, respectively. Moreover, Ca^{2+}-mediated cross-linking of homogalacturonan with low degree of esterification in the tube wall is crucial to pollen viability, as it stiffens the tube until cellulose and callose are deposited at the tube flanks to further strengthen the wall and maintain a unidirectional polarized growth (*26*). Labeling of the pollen tubes with *Pf*Avr4-2^{RR} showed that the protein localizes along the shank of the pollen tube walls but not at the growing tip, thus alluding to the specific binding of *Pf*Avr4-2 to fully or partially de-esterified pectin. In contrast, labeling of the tubes with *Pf*Avr4^{RR} did not show any binding of the protein along the pollen tube (Fig. 4B). *Pf*Avr4-2^{RR} induced bursting of the pollen tubes around the apical area in a [Ca^{2+}]-dependent manner, shortly after their exposure to the protein. Specifically, in the absence of Ca^{2+}, 86% of the pollen tubes burst within 2 hours of their exposure to the protein as compared to 18% of the pollen tubes bursting when exposed to *Pf*Avr4 or the pollen germination media alone. The addition of increasing amounts of $CaCl_2{\cdot}2H_2O$ to the pollen germination media resulted in an analogous gradual reduction in the percentage of pollen tubes bursting in the presence of *Pf*Avr4-2, whereas this effect was not seen in the presence of *Pf*Avr4 or the pollen germination media alone (Fig. 4B). Collectively, these results suggest that *Pf*Avr4-2 weakens the structural integrity of cell walls in pollen tubes in a [Ca^{2+}]-dependent manner, possibly by interfering with the Ca^{2+}-mediated cross-linking and formation of the egg-box structures in the pollen tubes.

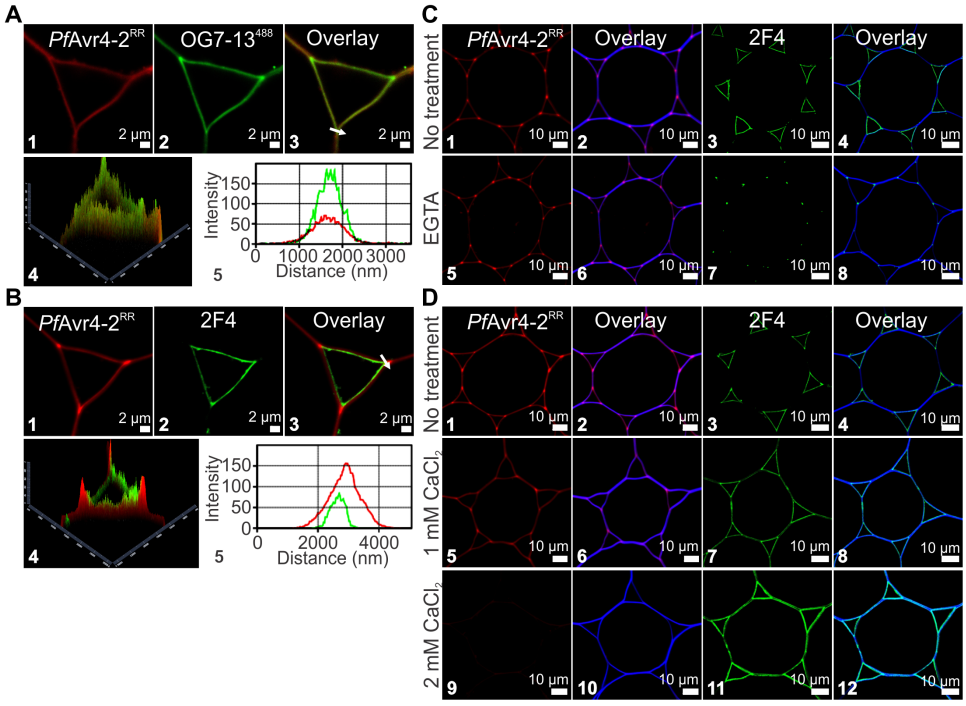

Fig. 3. *Pf*Avr4-2 competes with Ca^{2+} for binding to de-esterified homogalacturonan at junction zones. (**A**) Labeling of cross sections of *Arabidopsis* stems with *Pf*Avr4-2^{RR} and the OG7-13^{488} probe. *Pf*Avr4-2^{RR} is conjugated to the red fluorochrome Rhodamine Red (RR), whereas the OG7-13^{488} probe is conjugated to the green fluorophore Alexa Fluor 488. Cells are pith parenchyma, and labeling was performed sequentially with the two probes. Panel (A4) is a 2.5D representation of (A3), whereas the fluorescence intensities of *Pf*Avr4-2^{RR} and the OG7-13^{488} probe at the corner of the tricellular junction marked by an arrow in (A3) are shown in (A5). (**B**) Labeling of cross sections of *Arabidopsis* stems with *Pf*Avr4-2^{RR} and the 2F4 mAb. A secondary mAb conjugated to the green fluorophore Alexa Fluor 488 was used for detecting the 2F4 mAb. Cells are pith parenchyma, and labeling was performed sequentially with the two probes. Panel (B4) is a 2.5D representation of (B3), whereas the fluorescence intensities of *Pf*Avr4-2^{RR} and the 2F4 mAb at the corner of the tricellular junction marked by an arrow in (B3) are shown in (B5). (**C**) Labeling of cross sections of *Arabidopsis* stems with *Pf*Avr4-2^{RR}, the 2F4 mAb, or CW (blue signal) after pretreatment of the stems with the Ca^{2+} chelating agent EGTA. Cells are pith parenchyma. (**D**) Labeling of *Arabidopsis* stem cross sections with *Pf*Avr4-2^{RR}, the 2F4 mAb, or CW in increasing calcium concentrations ([Ca^{2+}]).

Stable expression of *PfAvr4-2* in tomato alters the plant's growth and textural properties

To examine whether *Pf*Avr4-2 could be interfering with Ca^{2+}-mediated cross-linking under in planta conditions, we generated two transgenic tomato lines of cv. Moneymaker that constitutively express under the control of the cauliflower mosaic virus 35*S* promoter (*CaMV* 35*S*), the mature form of *Pf*Avr4-2, fused to the PR1a secretion signal of *Nicotiana tabacum* for secretion into the apoplast. Primary transgenic plants were selected on kanamycin and two homozygous T_2 lines (i.e., 35*S*::*PfAvr4-2_1* and 35*S*::*PfAvr4-2_2*) obtained by segregation analysis of T_1 kanamycin-resistant plants were lastly selected for further analysis.

Quantification of transgene expression using quantitative polymerase chain reaction (qPCR) showed that *PfAvr4-2* expression levels were 5.92 times higher in the 35*S*::*PfAvr4-2_1* line as compared to the 35*S*::*PfAvr4-2_2* line (Fig. 5A). Notably, immunolabeling with the 2F4 monoclonal antibody of pectins extracted from leaves showed a substantially weaker and inversely correlated with the levels of *PfAvr4-2* expression, labeling of the pectin fraction obtained from the two 35*S*::*PfAvr4-2* transgenic lines than from the control Moneymaker line, suggesting reduced Ca^{2+}-mediated cross-linking in their plant cell walls. In contrast, labeling with the JIM5 monoclonal antibody showed no differences in signal intensity, indicating that pectin levels were similar among the three lines (Fig. 5B). To further investigate whether the stable expression of *Pf*Avr4-2 in tomato plants instigated any changes in the composition of the cell wall, leaf material from the two transgenic lines and the control Moneymaker line was subjected to comprehensive microarray polymer profiling (CoMPP) of major plant cell wall components using 21 unique anti-glycan monoclonal antibodies (fig. S5A) (*27*). The CoMPP analysis indicated that there were no substantial changes among the three lines in the signal intensities of the anti-homogalacturonan monoclonal antibodies JIM5 and JIM7. Signal intensities from antibodies that recognize the backbone of rhamnogalacturonan I (INRA-RU1) and its side chains (LM5 and LM6), xyloglucan (LM15 and LM25), and arabinogalactan (JIM13) were slightly decreased in the transgenic lines as compared to the control Moneymaker line, whereas the opposite was observed in signal intensities from antibodies recognizing epitopes of the hemicelluloses xylan (LM10) and arabinoxylan (INRA-AX1). However, with the exception of the change observed for arabinoxylan, all others were not significant at $\alpha = 0.05$ and were mostly observed in the NaOH fraction. Moreover, further monosaccharide composition analysis using high-performance anion-exchange chromatography with pulsed amperometric detection (HPAEC-PAD) indicated that the changes in the CoMPP profiles were not supported by any substantial changes in monosaccharide profile (fig. S5B), suggesting that they are either too small to yield any changes in monosaccharide content or/and that the results reflect changes in organization rather than amounts of cell wall polymers. Collectively, the above

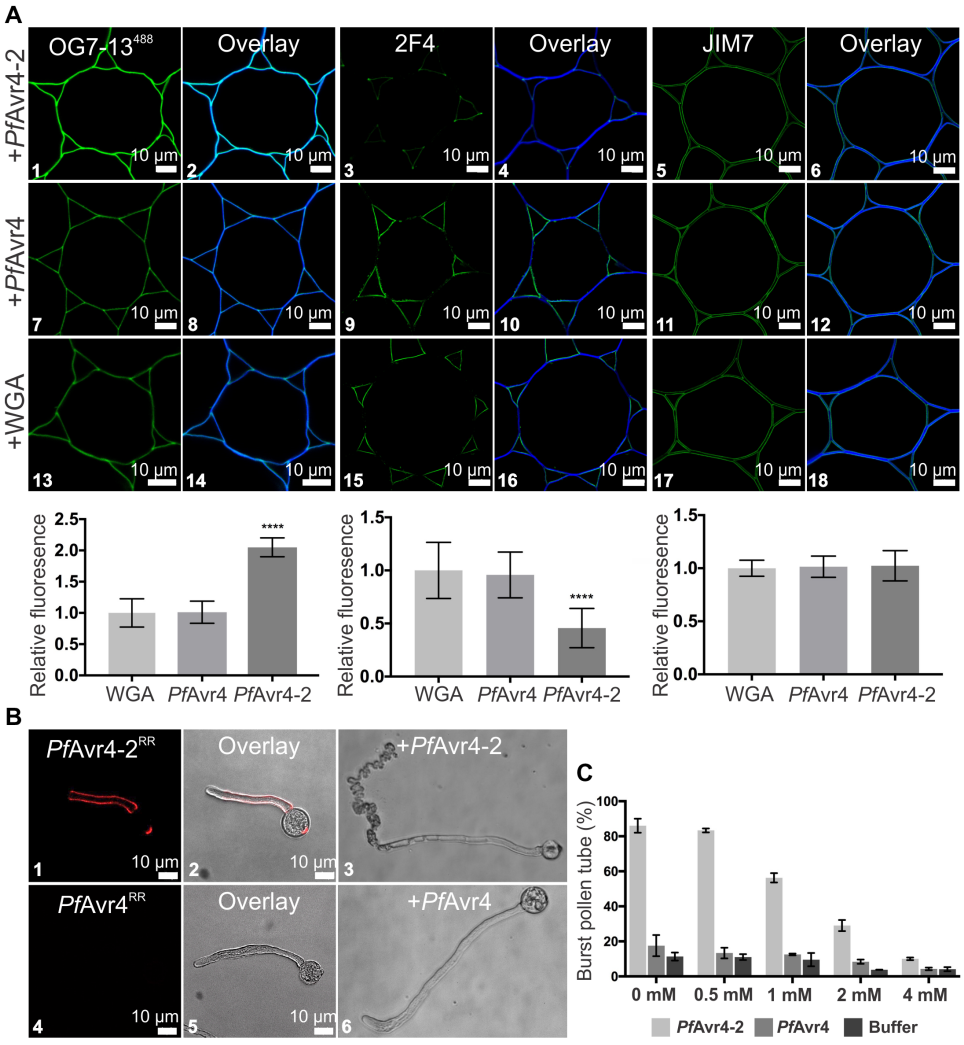

Fig. 4. *Pf*Avr4-2 can disrupt existing Ca^{2+}-mediated cross-links formed between adjacent homogalacturonan chains. (**A**) Labeling of cross sections of *Arabidopsis* stems with the OG7-13^{488} probe and the 2F4 and JIM7 monoclonal antibodies (mAbs) after pretreatment of the stems with 10 μM *Pf*Avr4-2, *Pf*Avr4, or WGA. The OG7-13^{488} probe is conjugated to the green fluorophore Alexa Fluor 488, whereas a secondary mAb also conjugated to Alexa Fluor 488 was used for detecting the 2F4 and JIM7 mAbs. Cells are pith parenchyma. Labeling with the OG7-13^{488} probe necessitates the addition of 1 mM Ca^{2+} in the labeling buffer. Bottom graphs show the fluorescence intensity of the OG7-13^{488} probe, the 2F4, and JIM7 mAbs, relative to WGA (signal set to 1.0). Error bars indicate SD (OG7-13^{488}, $n = 15$; $2F4^{488}$, $n = 20$; JIM7, $n = 12$). Statistical differences between *Pf*Avr4-2 and other treatments were determined by ANOVA using Tukey's test. ****$P < 0.0001$. (**B**) Microscope images of germinating pollen tubes of tomato incubated at increasing calcium concentrations ([Ca^{2+}]) with *Pf*Avr4-2^{RR} or *Pf*Avr4^{RR} conjugated to the red fluorochrome Rhodamine Red (RR). Shown are the images where 1 mM $CaCl_2{\cdot}2H_2O$ was used in the labeling buffer. (**C**) Effect of *Pf*Avr4-2, *Pf*Avr4, and a buffer control under increasing [Ca^{2+}] on bursting of tomato pollen tubes. The experiment was repeated in triplicate, and 100 pollen tubes were counted in each of the replicates. Error bars indicate SD from three replicates.

results suggest that the stable expression of *Pf*Avr4-2 in tomato plants does not lead to any major changes in the composition of the plant cell wall other than reducing their Ca^{2+}-mediated cross-linking.

Further phenotypic analysis of the transgenic plants indicated that the reduction in Ca^{2+}-mediated cross-linking is accompanied by changes in their morphological, anatomical, and textural properties that are associated with relaxation in plant cell wall stresses. Transgenic plants had elongated stems and were taller as compared to the control Moneymaker ones (Fig. 5C), whereas fewer but larger in size cortical cells were observed in their stems that likely contributed to their increase in length (Fig. 5D). As Ca^{2+}-mediated cross-linking of homogalacturonan in plant cell walls confers mechanical strength to the plant tissue (*7*), characterization of the plants' textural properties via an indentation tested on the plants' petioles using a texture analyzer (Fig. 6A) showed that the 35*S::PfAvr4-2*–expressing plants were softer as compared to the control Moneymaker plants (Fig. 6B). Specifically, compared to the control Moneymaker plants, the 35*S::PfAvr4-2*–expressing plants offered less resistance to indentation, as the maximum force on the probe achieved during the test was significantly lower for the transgenic lines. Stiffness of the petiole tissue, defined as the maximum force achieved during the test divided by the total distance traveled by the probe, was also lower for the transgenic lines than for the Moneymaker line. Last, the distance at fracture, quantified as the displacement of the probe when the first significant fracture (breakage) of the tissue occurred, was again greater for the transgenic lines than for the Moneymaker

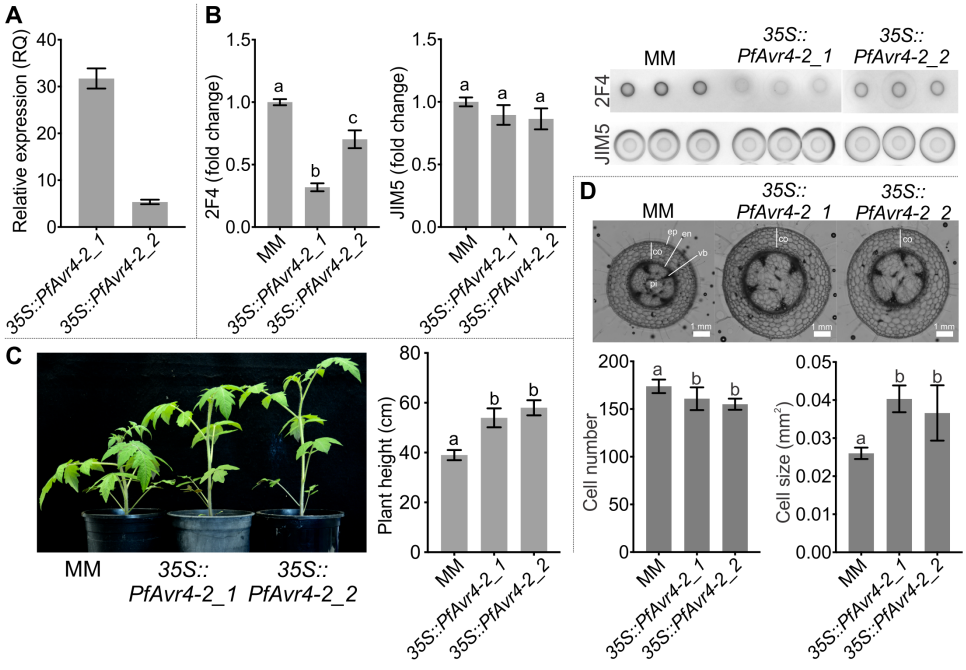

Fig. 5. The 35*S::PfAvr4-2* transgenic tomato plants have altered anatomical characteristics. (**A**) *PfAvr4-2* expression levels in the two 35*S::PfAvr4-2* tomato lines (35*S::PfAvr4-2_1* and 35*S::PfAvr4-2_2*), relative to the tomato *RLP2* gene (set to 1.0 RQ). Error bars indicate SD from six samples. (**B**) immunodot blot analysis of Ca^{2+}-mediated cross-linked homogalacturonan and of pectin extracted from the cell walls of 6-week-old plants. An equal amount of 33 μg of Ca^{2+}-mediated cross-linked homogalacturonan or of pectin was spotted on each dot and probed with the 2F4 or JIM5 monoclonal antibodies, respectively. Bars indicate signal intensity, error bars are SD from minimum nine spots per line, and letters are significant differences based on a Tukey's test ($\alpha = 0.05$). (**C**) Height of 6-week-old 35*S::PfAvr4-2* and control cv. Moneymaker (MM) plants. Bars represent the average height of seven plants per line, error bars are SD, and letters are significant differences based on a Tukey's test ($\alpha = 0.05$). (**D**) Cell size and cell number comparisons between the 35*S::PfAvr4-2* and control Moneymaker plants in stem cross sections made at 1 cm from the crown base. Main anatomical features are indicated; ep, epidermis; co, cortex; en, endodermis; vb, vascular bundle (xylem-cambium-phloem); pi, pith. Bars represent the average cell number or size in the cortex of 2-week-old plants per line. Cell numbers were quantified by measuring the number of the cells in the cortex of seven plants, and cell size was quantified by measuring the area of the cortex and dividing it by the number of cells. Error bars indicate SD and letters are significant differences based on a Tukey's test ($\alpha = 0.05$). Photo credit: Li-Hung Chen, University of California, Davis.

line (Fig. 6B). This parameter showed that the petiole tissue from the transgenic plants was both softer and more compliant than the Moneymaker plants, as it could be deformed to a greater extent before fracturing.

*Pf*Avr4-2 contributes to virulence by enhancing the activity of a fungal endo-PG

Since *Pf*Avr4-2 interferes with the integrity of the plant cell walls, we next examined whether this activity contributes to fungal virulence. Virulence assays performed with the wild-type *P. fuligena* on the two the two 35*S::PfAvr4-2*–expressing lines and the control Moneymaker line indicated that the fungus induced considerably more necrosis (Fig. 7, A and B) and accumulated more biomass (Fig. 7C) in inoculated leaves of the two transgenic lines as compared to the Moneymaker line. Similarly, spot inoculations with the necrotrophic pathogen *Botrytis cinerea* on leaves of the two transgenic lines and the control Moneymaker line also showed that the diameter of the infection lesions was significantly larger in the former (Fig. 7, D and E). To further confirm that *Pf*Avr4-2 is a virulence factor, we examined whether it is expressed under in planta conditions and whether its deletion from the genome of *P. fuligena* would have an effect on fungal infectivity. Analysis of the in planta expression of *PfAvr4-2*, showed that it exhibits a transient expression pattern in which transcription is steadily increased during the initial biotrophic stage of the infection (1 to 6 days post inoculation), reaching a maximum at the time of transitioning from biotrophy to necrotrophy (8 to 9 days after inoculation) and gradually decreasing thereafter (Fig. 7F). Virulence assays with two *PfAvr4-2* deletion mutants (Δ*Pf*Avr4-2_1 and Δ*Pf*Avr4-2_2) that were generated showed that relative to the wild-type *P. fuligena* strain, the two Δ*PfAvr4-2* mutants induced less symptoms and produced less biomass in leaves of infected Moneymaker plants (Fig. 7, G and H). Collectively, these results support that *Pf*Avr4-2 is a virulence factor.

We next sought to investigate how *Pf*Avr-4-2 could be contributing to fungal virulence. Ca^{2+}-mediated cross-linking of homogalacturonan chains increases cell-cell adhesion, which, in turn, may further limit hydrolyzing enzymes from accessing the plant cell wall (*7*, *28*). We thus used the PECTOPLATE assay (*29*) to examine whether by interfering with Ca^{2+}-mediated cross-linking in plant cell walls, *Pf*Avr4-2 could be affecting the enzymatic activity of various homogalacturonan-modifying enzymes, including PMEs from *B. cinerea*, an endo-PG from *Aspergillus niger*, an exo-PG from *Yersinia enterocolitica* (exo-PG), and a pectate lyase from *Aspergillus* sp. Mixing of *Pf*Avr4-2 with the endo-PG resulted in an ~46% increase relative to controls in the diameter of the cleared halo formed around the wells containing the mixture, indicating that *Pf*Avr4-2 enhanced the activity of this enzyme (Fig. 8A). The increase in the diameter of the halo was caused by the endo-PG, as *Pf*Avr4-2 did not

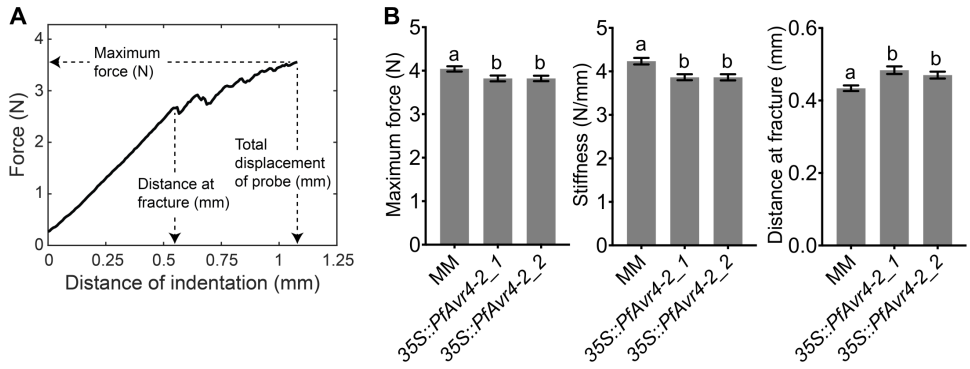

Fig. 6. The 35*S::PfAvr4-2* transgenic tomato plants have altered textural characteristics. (**A**) Exemplary texture curve showing the parameters that were defined using texture analysis. The textural properties of the petioles were tested by an indentation test. Parameters measured were "maximum force (in newton)," which refers to the maximum normal force exerted by the petiole on the probe during the test; "distance at fracture (in millimeter)," which refers to the displacement of the probe when the first significant fracture (breakage) of the tissue occurred; and "stiffness (in newton per millimeter)," which refers to the maximum force (in newton) achieved during the test divided by the total distance traveled by the probe (in millimeter) (achieved at 33% strain). (**B**) Textural properties of the two 35*S::PfAvr4-2*–expressing lines (35*S::PfAvr4-2_1* and 35*S::PfAvr4-2_2*) and the control cv. Moneymaker (MM) tomato line, as measured with the indentation test. Bars show that maximum force and stiffness, which positively correlate with tissue firmness, and the distance at fracture, which indicates the extent to which the tissue can be deformed before fracture occurs. Error bars indicate SD and were obtained from performing indentation tests at four equally distanced sites per petiole. At least 29 petioles were tested for each line (resulting in a minimum of 115 total compression tests per line). Letters show significant differences based on a Tukey's test ($\alpha = 0.05$).

show any pectin-related enzymatic activity (Fig. 8B). The positive impact of *Pf*Avr4-2 on the activity of the endo-PG was further confirmed by a spectrophotometric enzyme activity assay that quantified the OGs released from degradation of homogalacturonan in the presence/absence of *Pf*Avr4-2 (Fig. 8C). In contrast to endo-PG activity, there were no changes relative to controls in the pattern or diameters of the fuchsia-colored haloes formed around wells containing mixtures of *Pf*Avr4-2 with the PME, exo-PG, or pectate lyase (fig. S6A). In contrast, *Pf*Avr4 and WGA had no impact on the activity of the endo-PG, indicating that the effect seen with *Pf*Avr4-2 was specific (fig. S6B).

*Pf*Avr4-2 does not suppress OG-induced immunity in tomato and is not recognized by Cf-4

As OGs can be perceived as DAMPs, thereby eliciting immune responses (*12*), we examined whether *Pf*Avr4-2 has the ability to suppress OG-triggered immunity, as demonstrated for other carbohydrate-binding effectors (*30*). However, treatment of the two 35*S::PfAvr4-2*–expressing lines and the control Moneymaker line with 100 μM OG10-15 solution did not result in statistically significant differences among the three lines in the accumulation of reactive oxygen species (ROS), indicating that *Pf*Avr4-2 is unable to inhibit the OG-induced ROS burst in tomato (fig. S7A). Last, since effectors may mediate avirulence in the presence of cognate resistance genes, we examined whether *Pf*Avr4-2 is perceived by the Cf-4 immune receptor from tomato that mediates HR upon recognition of Avr4 proteins, including of *Pf*Avr4 (*19*). Transient coexpression of *PfAvr4* or *PfAvr4-2* with *Cf-4* in *N. tabacum* and *Nicotiana benthamiana* using an *Agrobacterium tumefaciens* transient transformation assay showed that only *Pf*Avr4 induced HR in the presence of the Cf-4 receptor, thus suggesting the lack of *Pf*Avr4-2 recognition by Cf-4 (fig. S7B). However, lack of an anti–*Pf*Avr4-2 antibody impeded us from testing whether the absence of a HR was due to the lack of protein accumulation in the infiltrated tissue.

DISCUSSION

Here, we show that a candidate effector from the tomato pathogen *P. fuligena* assists infections by binding to homogalacturonan with a low degree of esterification in the plant's middle lamella or the primary cell wall and interfering with the Ca^{2+}-mediated cross-linking of homogalacturonan chains. This, in turn, loosens the plant cell wall and synergizes the activity of fungal endo-PGs (fig. S8).

Carbohydrate-binding modules are generally known to synergize the activity of appending CAZymes by promoting the interaction of the enzyme with the target substrate and/or through the noncatalytic disruption of the substrate (*31*). It is shown, for example, that cellulose-binding domains enhance the activity of cellulases by sliding like a wedge and thus disrupting the hydrogen bonding between two adjacent cellulose chains, thereby enabling the enzyme to penetrate more deeply into crystalline cellulose (*32*). Through binding to nonmethylated GalA residues in intermittently Ca^{2+}-mediated cross-linked homogalacturonan chains, *Pf*Avr4-2 could likewise part adjacent homogalacturonan chains and disrupt their Ca^{2+}-mediated cross-linking, thus providing endo-PGs better access to unesterified regions of homogalacturonan and creating more cleavage sites along the homogalacturonan backbone (fig. S8). Notably, endo-PGs are most active against homogalacturonan with a low degree of esterification, and therefore, they often function in cohort with pathogen secreted PMEs (*33*, *34*). As primary cell walls consist of a matrix of cellulose microfibrils associated with pectins and hemicelluloses (*35*), the enhanced destruction of the pectin network could subsequently indirectly aid the enzymatic degradation of other plant cell wall–based polysaccharides, thus further accelerating the decomposition of the plant tissue. This may also explain why *Pf*Avr4-2 exhibits higher expression levels during the switch to the necrotrophic phase rather than the initial biotrophic phase, as is the case with many effectors (*16*). Plants, on the other hand, are also known to tightly regulate the degree and pattern of pectin methylesterification during host-microbe interactions through the precise and timely activation of endogenous PMEs and PME inhibitors.

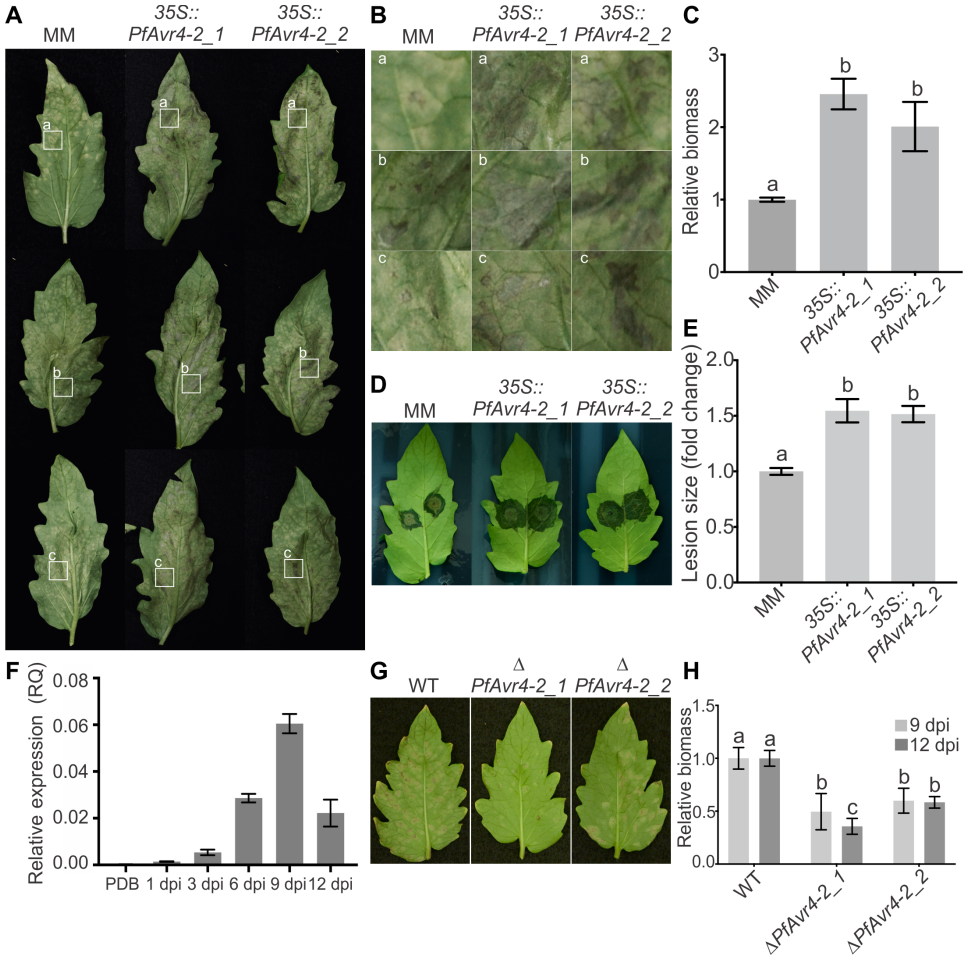

Fig. 7. *PfAvr4-2* is a virulence factor. (**A**) Disease symptoms at 15 days post inoculation (dpi) induced by *P. fuligena* on leaves of the 35*S*::*PfAvr4-2* tomato lines (35*S*::*PfAvr4-2_1* and 35*S*::*PfAvr4-2_2)* and the control cv. Moneymaker (MM) line. (**B**) Magnification of the sections marked by white boxes in (A). (**C**) Quantification (9 dpi) of *P. fuligena* biomass in leaves of the 35*S*::*PfAvr4-2* plants relative to its biomass in leaves of Moneymaker (set to 1.0). Error bars indicate SEM from three assays and letters significant differences based on a Tukey's test ($\alpha = 0.05$). (**D**) Infection lesions (3 dpi) of *B. cinerea* on leaves of Moneymaker and 35*S*::*PfAvr4-2* plants. (**E**) Mean diameter of the infection lesions produced on the 35*S*::*PfAvr4-2* plants relative to the Moneymaker line (set to 1.0). Error bars indicate SD in lesion diameters from three assays and ten leaves per line. Letters show significant differences based on a Tukey's test ($\alpha = 0.05$). (**F**) In vitro and in planta *PfAvr4-2* expression levels, relative to the *P. fuligena GAPDH* gene (set to 1.0 RQ). Shown are average RQ values from two inoculation assays on the Moneymaker line. Error bars indicate SE from four qPCRs. (**G**) Virulence (15 dpi) of a wild-type (WT) *P. fuligena* and of two *PfAvr4-2* deletion mutants (Δ*PfAvr4-2_1* and Δ*PfAvr4-2_2*) on Moneymaker plants. (**H**) Quantification of fungal biomass in tomato leaves infected with the Δ*PfAvr4-2* mutants, relative to the biomass of the wild-type (WT) strain (set to 1.0 RQ). Error bars indicate SEs from three virulence assays. Letters show significant differences based on a Tukey's test ($\alpha = 0.05$). Photo credit: Li-Hung Chen, University of California, Davis.

Overexpression of PME inhibitors, for example, is shown in various plant species to increase resistance against necrotrophic and hemibiotrophic pathogens, owing to the reduced susceptibility of methyl-esterified pectin to pectic enzymes secreted by pathogens. As the status of pectin methyl-esterification is also crucial to *Pf*Avr4-2's function, it is plausible that PME inhibitors further promote resistance by indirectly interfering with the protein's activity. Decreased binding of *Pf*Avr4-2 to plant cell walls was observed in the tomato PME-silencing lines, suggesting that PME inhibitors would negatively affect the virulence function of *Pf*Avr4-2. Thus, by reducing the levels of pectin methyl-esterification, PME inhibitors lower both pectin's susceptibility to enzymatic digestion and its amenability by *Pf*Avr4-2.

The disruption by *Pf*Avr4-2 of the Ca^{2+}-mediated cross-links in plant cell walls could also loosen their structure, a function that is somewhat reminiscent of the function of expansins. Expansins are a large superfamily of mainly plant proteins that mediate the non-catalytic loosening of the cell wall by disrupting hydrogen bonds linking adjacent wall polysaccharides and thus reducing their adhesion (*36*). Despite the lack of sequence similarity between *Pf*Avr4-2 and known expansins of plant or microbial origin, there are interesting similarities between the function of the two groups. For instance, they both act on noncovalent bonds and are most active at acidic pH. They also lack lytic activity on polysaccharide substrates while mediating the reversible disruption of cross-links between adjacent polysaccharide chains, thus reducing their adhesion and loosening the cell wall. However, *Pf*Avr4-2 does not interact with cellulose, a nearly universally property in plant and microbial expansins and has a CBM14 domain instead of the typical CBM63 cellulose-binding domain and family 45 glycosyl hydrolase (GH45) domain found in canonical expansins (*36*).

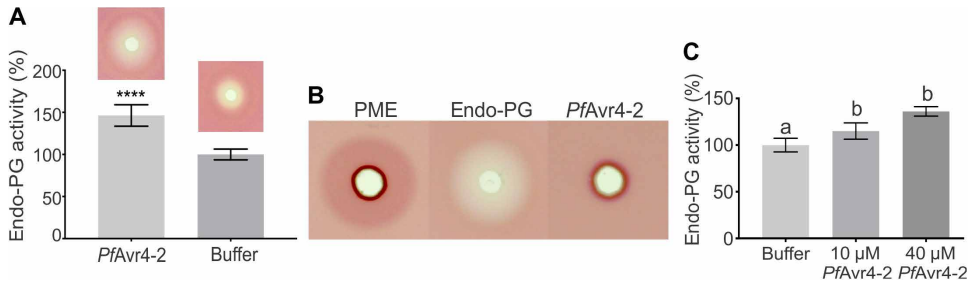

Fig. 8. *PfAvr4-2* enhances the activity of fungal endo-PGs. (**A**) Relative quantification of fungal endo-PG activity in the presence of *Pf*Avr4-2 using the PECTOPLATE. The bar graph shows relative quantification based on the intensity of Ruthenium Red staining around the inoculation wells of endo-PG activity when the enzyme is applied alone or in a mixture with *Pf*Avr4-2. Experiments were done in triplicate, and the intensity of the fuchsia-colored halo produced by the activity of the endo-PG is set to 100%. Error bars indicate SD from the three experiments. Student's *t* test was used to evaluate statistical significance of the difference between the two treatments. ****$P < 0.001$. The images above the bars provide a visual representation of the results. (**B**) Visual representation of the PECTOPLATE radial diffusion assay used to compare the pectin-related enzymatic activity of PME, endo-PG, and *Pf*Avr4-2. The enzymatic activity of the three pectin-related proteins is assessed on the basis of the size of the fuchsia-stained haloes in the PECTOPLATE. (**C**) Relative quantification of endo-PG activity in the presence of increasing amounts of *Pf*Avr4-2. The enzymatic activity of endo-PG was monitored by measuring using 2-cyanoacetamide, the amount of oligogalacturonides (OGs) released in the buffer. The activity of endo-PG alone was set to 100%, and the activity of the enzyme in mixtures with different amounts of *Pf*Avr4-2 was expressed relative to this activity. Experiments were done in triplicate, and error bars indicate SD. Treatments with the same letter were not significantly different by a Tukey's test ($\alpha = 0.05$).

Although chitin is the only known binding substrate of CBM14 modules, *Pf*Avr4-2 is an exception as it interacts with pectin in plant cell walls. This finding expands the substrate specificity of the CBM14 family and further broadens the role of fungal apoplastic effectors in structural modification of plant cell walls. Other examples of effectors that fulfill their role in virulence through carbohydrate binding include the chitin-binding Avr4 (*17*, *19*) and Ecp6 (*30*) core effector proteins that protect fungal chitin against chitinases or inhibit chitin-induced innate immunity by sequestering chito-oligosaccharides from the apoplastic space and the FGB1 effector from *Piriformospora indica* that suppresses β-glucan–triggered innate immunity by binding to β-glucans released from the fungal cell wall (*37*). These examples show that microbial lectins can serve multiple virulence roles as effectors during infections, including protection or noncatalytic disruption of polysaccharide substrates, enhancement of the hydrolytic activity of cell wall–degrading enzymes, and subversion of plant defense responses. Such functions may be particularly important for extracellular pathogens, as the carbohydrate-rich plant and fungal cell walls form the main interface of interaction between plants and pathogens in the apoplast and are consequently reciprocally targeted by each side seeking to gain an advantage.

MATERIALS AND METHODS

Plant materials and growth conditions

Tomato plants were grown in the growth chamber with 16-hour light and 70% relative humidity at 25°C for 6 weeks. *Arabidopsis thaliana* plants were grown in a controlled environment chamber with a 10-hour photoperiod at 23°C and 75% relative humidity.

Allelic variation

Allelic variation was examined in 30 strains of *P. fuligena* originating from Taiwan ($n = 1$) and nine prefectures of Japan, i.e., Aichi ($n = 1$), Chiba (n = 2), Fukuoka ($n = 1$), Gifu ($n = 6$), Mie ($n = 14$), Shizuoka ($n = 1$), Tokushima ($n = 2$), Tottori (n = 1), and Wakayama ($n = 1$). Genomic DNA was extracted from the strains using the DNeasy Plant Mini Kit (QIAGEN), and the *PfAvr4-2* gene was amplified with primers *Pf*Avr4-2_F1/*Pf*Avr4-2_1 (table S1) using the REDTaq DNA Polymerase (Sigma-Aldrich). PCR reaction cycle consisted of an initial 95°C for 10 min, followed by 15 s at 95°C, 30 s at 58°C, and 30 s at 72°C for 40 cycles. PCR products were sequenced with primer *Pf*Avr4-2_R2 (table S1), and obtained electropherograms were aligned using the MEGA software package (v6.0) (*38*).

Protein structure modeling

The 3D model of *Pf*Avr4-2 was generated by I-TASSER (Iterative Threading ASSEmbly Refinement) with the default settings (https://zhanglab.ccmb.med.umich.edu/I-TASSER/) (*39*) and using the *Pf*Avr4 [Protein Data Bank (PDB): 4Z4A] and *Cf*Avr4 (PDB: 6BN0) structures as threading templates. The highest *C*-score (=0.14) model was used for further analysis. Protein structure alignments and coloring of the electrostatic surfaces and of o the side chains of Avr4 proteins were conducted using UCSF Chimera (v1.14) (*40*).

Protein purification from culture filtrates of *Pichia pastoris*

Recombinant *Pf*Avr4-2 protein was produced using the methylotrophic yeast *P. pastoris* GS115 as described by Kohler *et al.* (*19*). The produced by *Pf*Avr4-2 protein was purified through a NiNTA column (Thermo Fisher Scientific). The protein was eluted in 50 mM tris-HCl (pH 7.0) and 50 mM NaCl with 250 mM imidazole and concentrated in a Amicon Ultra-15 centrifugal filter unit (3-kDa cutoff; Millipore). The concentrated protein was further purified by passing through a Superdex 75 column (GE Healthcare) with 25 mM tris-HCl (pH 7.0) and 50 mM NaCl on an AKTA FPLC system (GE Healthcare; software UNICORN 5.2). The eluted protein was subsequently analyzed by a MiniDAWN TREOS MALS detector (Wyatt Technology) with a laser source at 658.8 nm, followed by an Optilab T-rEX refractometer (Wyatt Technology) with a 658.0-nm light source. The final protein was verified by SDS–polyacrylamide gel electrophoresis, concentrated, and stored at −80°C.

In vitro polysaccharide precipitation assays and fungal protection assays against chitinases

Binding assays of *Pf*Avr4-2 or *Pf*Avr4 with various insoluble polysaccharides that are common constituents of fungal and plant cell walls—such as shrimp-shell chitin (Sigma-Aldrich), colloidal chitin (Sigma-Aldrich), chitosan (Sigma-Aldrich), curdlan AL (InvivoGen), cellulose (Sigma-Aldrich), and xylan (Sigma-Aldrich)—were performed at three pHs (5.5, 7.0, and 8.5) as described previously (*17*, *19*), with some modifications (Supplementary Materials and Methods). To test whether *Pf*Avr4-2 can protect fungal hyphae against chitinases of tomato or bacterial origin, we followed the procedure described before (*17*, *19*) with some modifications (Supplementary Materials and Methods).

Defined carbohydrate microarray

The defined carbohydrate microarray was prepared as described before (*25*). Briefly, the carbohydrates were printed on a nitrocellulose membrane using a microarray printer (ArrayJet, Roslin, UK). *Pf*Avr4-2 was conjugated with fluorescein isothiocyanate (FITC; Thermo Fisher Scientific) following the manufacturer's protocol. The array was blocked with 5% bovine serum albumin (BSA) dissolved in a NaOAc/NaCl buffer [25 mM NaOAc and 50 mM NaCl (pH 5.5)] and incubated with *Pf*Avr4-2FITC at a 1:100 dilution for 1 hour at 4°C. The array was then washed twice with the NaOAc/NaCl buffer and scanned by a GenePix scanner using a 488-nm laser. The intensity of the fluorescence signals on the array was quantified using ProScanArray Express-MicroArray Analysis System software (v4.0.0.0004, PerkinElmer), and values were normalized from 0 to 100. Highest value was set as 100, and the cutoff value was 5. The experiment was performed once.

Isothermal titration calorimetry

For the ITC assays, *Pf*Avr4-2 was dialyzed against the NaOAc/NaCl buffer at 4°C for 2 days. The OG10-15 mixture (Carbosynth, catalog no. OG59704) was dissolved in the same buffer to a final concentration of 2 mM. ITC experiments were conducted on a NanoITC (TA Instruments). The heat change was quantified by titrating 2.5 μl of 2 mM OG10-15 into the cell containing 0.5 mM *Pf*Avr4-2 in a total volume of 170 μl with a 1.5-min equilibration time and a stir rate of 250 rpm for 20 titrations. Data were analyzed using the NanoITC analysis software (v3.7.5, TA Instruments) and fit with an independent binding model provided by the software. The first titration was done with 1 μl of 2 mM OG10-15, and the value of this point was used for fitting the model. ITC experiments were repeated twice with reproducible results.

Localization studies on fungal and plant cell walls

Localization of *Pf*Avr4 and *Pf*Avr4-2, labeled with Alexa Fluor 488 succinimidyl ester (488) (Life Technologies) or RR-X, succinimidyl ester (RR) (Life Technologies), respectively, on cell walls of *T. viride* was examined as described before (*19*). The experiment was repeated three times, and protein localization on fungal cell walls was examined on at least 30 germlings of *T. viride* with reproducible results. Localization of *Pf*Avr4 and *Pf*Avr4-2 on cell walls of *P. fuligena* was performed in a similar way (*19*), with some modifications. Specifically, mycelia of *P. fuligena* were first treated at 25°C for 1 hour with 5 U of Zymolyase (Zymo Research, catalog no. E1004) to remove the β-glucan layer in the fungal cell wall and expose the underlying chitin layer. The mycelia were then incubated with 3 μM *Pf*Avr4^{RR} or *Pf*Avr4-2^{RR} in the NaOAc/NaCl buffer at room temperature for 40 min. After washing three times with the same buffer, the fluorescent signal was detected with a Zeiss LSM710 confocal microscope using the 40× water objective. The experiment was repeated three times with reproducible results.

Localization studies of *Pf*Avr4^{488}, *Pf*Avr4-2^{488}, and *Pf*Avr4-2^{RR}; the OG7-13^{488} probe; and the JIM7 and 2F4 (PlantProbes, http://plantprobes.net) antibodies on *Arabidopsis* stem cross sections were done according to Mravec *et al.* (*25*), with modifications. All localization experiments on *Arabidopsis* stem cross sections were repeated at least three times with reproducible results. In each experiment, a minimum of two stem cross sections were labeled with the individual proteins or antibodies, and at least five pictures were taken per stem cross section. The *Arabidopsis* stem samples were collected at 2 cm above the leaf of 1-month-old *Arabidopsis* plants and fixed in 4% formaldehyde for 1 hour at room temperature. After washing with water, the stem samples were embedded in 5% agarose and sectioned into 150-μm-thick sections using a Vibratome-1000. The stem cross sections were then washed three times with the NaOAc/NaCl buffer and 2 μM of the assayed proteins was incubated with the sections in 500 μl of the same buffer for 40 min. CW (50 μg/ml) (Sigma-Aldrich) was used for labeling cellulose in plant cell walls on the stem cross sections for 10 min at room temperature. After washing three times with the NaOAc/NaCl buffer, the fluorescence signal was detected with a Zeiss LSM710 confocal microscope using the 40× water or 63× oil objectives. Images were analyzed using the Zen imaging software (v2.3, blue edition, ZEISS).

For immunostaining of the *Arabidopsis* stem cross sections with the JIM7 and 2F4 monoclonal antibodies, the antibodies were diluted 1:50 in the NaOAc/NaCl buffer and incubated with the stem samples for 1 hour at room temperature. After washing with the NaOAc/NaCl buffer three times, anti-rat immunoglobulin G (IgG; H + L) secondary monoclonal antibody with Alexa Flour 488 (A-11006, Invitrogen) was used for detecting the JIM7 monoclonal antibody, whereas anti-mouse IgG (H + L) secondary monoclonal antibody with Alexa Flour 488 (A28175, Invitrogen) was used for detecting the 2F4 monoclonal antibody. The secondary antibodies were diluted 250× in the NaOAc/NaCl buffer and mixed with the samples for 1 hour at room temperature. For labeling of the stem samples with the OG7-13^{488} probe, 2 μM probe was incubated with the *Arabidopsis* stem cross sections in the NaOAc/NaCl buffer that also contained 1 mM $CaCl_2$. The fluorescence intensity of images was analyzed and quantified using the Zen imaging software (v2.3, blue edition, ZEISS).

To localize *Pf*Avr4-2^{RR} and *Pf*Avr4^{488} on tomato leaves infected with *P. fuligena*, the leaves of 6-week-old Moneymaker tomato plants were inoculated with the mycelial fragments of the wild-type *P. fuligena* strain as described before (*19*). The infected tomato leaves were collected at 9 days after inoculation and washed with 100% ethanol for 2 days to remove all chlorophyll. The samples were subsequently washed with the NaOAc/NaCl buffer and labeled with *Pf*Avr4-2^{RR} and *Pf*Avr4^{488}, as described above. Images were taken with a Zeiss LSM710 microscope using 63× oil objective and analyzed with the Zen imaging software (v2.3, blue edition, ZEISS). The experiment was repeated three times with reproducible results, and at least ten images were taken from two infected leaves in each experiment.

The PME-silenced tomato lines (cv. Rutgers) were a gift from E. Mitcham in the Department of Plant Sciences, UC Davis. Tomato

stems ($n = 2$) from 5-week-old tomato plants were embedded, sectioned, and labeled with *Pf*Avr4-2^{RR} as described above for *Arabidopsis* stems. Images ($n = 5$ per stem) of tomato stems stained with *Pf*Avr4-2^{RR} were taken with a Zeiss LSM710 microscope using 20× and 40× water objectives and analyzed with the Zen imaging software (v2.3, blue edition, ZEISS). The experiment was repeated three times with reproducible results.

Enzymatic and chemical treatment of *Arabidopsis* stem cross sections

To investigate how pH and calcium concentration ($[Ca^{2+}]$) influence the localization of *Pf*Avr4-2 on plant cell walls, *Arabidopsis* stem cross sections ($n = 6$ per treatment) were incubated for 40 min at room temperature with 2 μM *Pf*Avr4-2^{RR} in a NaOAc/NaCl buffer and a tris-HCl/NaCl solution (25 mM tris-HCl and 50 mM NaCl) buffered at pH 7.0 and pH 8.5 as well as the NaOAc/NaCl buffer supplemented with 1 and 2 mM $CaCl_2$. After washing the samples with the same buffers, images ($n = 5$ per stem cross section per treatment) of the stem cross sections were taken with a Zeiss LSM710 confocal microscope and analyzed using the Zen imaging software (v2.3, blue edition, ZEISS). For the pectinase, NaOH, and EGTA treatments, *Arabidopsis* stem cross sections ($n = 6$ per treatment) were pretreated with 8 mU of a fungal pectinase mix consisting of pectin transeliminase, PG, and pectin esterase (Sigma-Aldrich, catalog no. P2736). Treatments were done at room temperature in 100 mM NaOH for 2 hours or 50 mM EGTA for 15 min in a total volume of 500 μl of the NaOAc/NaCl buffer. After treatment, the samples were washed three times with the same buffer and then probed with *Pf*Avr4-2^{RR}, as described above. Images ($n = 5$ per stem cross section per treatment) were taken with the Zeiss LSM710 microscope using 20× and 40× water objectives and were analyzed with the Zen imaging software (v2.3, blue edition, ZEISS). The experiment was repeated three times with reproducible results.

Monitoring the state of Ca^{2+} cross-links (i.e., egg boxes) in junction zones

Stem segments of 1-month-old *Arabidopsis* plants were embedded in 5% agarose and thin sectioned using a Vibratome-1000. The thin cross sections were then incubated for 2 hours with 10 μM *Pf*Avr4, *Pf*Avr4-2, or WGA in 500 μl of the NaOAc/NaCl buffer. To label them with the OG7-13^{488} probe, the stem cross sections ($n = 3$ per pretreatment) were washed three times with the NaOAc/NaCl buffer, and then 2 μM OG7-13^{488} probe dissolved in the same buffer containing 1 mM $CaCl_2$ was added to the samples. To label the stem cross sections with the 2F4 monoclonal antibody, the sections ($n = 3$ per pretreatment) were first washed with the NaOAc/NaCl buffer for 1 hour to remove *Pf*Avr4-2, *Pf*Avr4, or WGA and then immunostained in the same buffer with the 2F4 monoclonal antibody and the anti-mouse IgG (H + L) secondary monoclonal antibody conjugated to the Alexa Fluor 488. After washing three times with the NaOAc/NaCl buffer, images ($n = 5$ per stem cross section per treatment) were taken with a Zeiss LSM710 confocal microscope using a 40× water lens or 63× oil lens and analyzed with the Zen imaging software (v2.3, blue edition, ZEISS). Quantification of relative fluorescence was done by measuring the fluorescence signal at the corners of cell junction from more than 12 images using the Zen software (Zeiss). The fluorescence intensity of 2F4 or OG7-13^{488} labeling after WGA treatment was set to 1.0 for calculating the relative fluorescence of other treatments. Experiments were performed three times with reproducible results. Statistical analysis was performed with the GraphPad Prism software (v8.3.1., Graphpad software Inc.). Student's *t* test was conducted to evaluate the significance of difference among treatments.

Pollen tube assays

The germination of pollen tubes in pollen germination media was examined as described before (*41*). Briefly, fully open flowers of young Moneymaker tomato plants were collected into 2-ml tubes containing 1 ml of pollen germination media buffer [24% (w/v) polyethylene glycol 4000, 0.01% (w/v) H_3BO_3, 2% (w/v) sucrose, 20 mM Hepes buffer (pH 6.0), 0.02% $MgSO_4$, and 1 mM KNO_3]. The tubes were then gently vortexed for 15 s to release the pollen grains from flowers. Pollen grains (500 grains/ml) were pregerminated in pollen germination media buffer amended with $CaCl_2$ at different concentrations (0, 0.5, 1, 2, and 4 mM) in a 48-well plate for 1 hour at room temperature. A 20 μM *Pf*Avr4 or *Pf*Avr4-2 was then added into each well in a total volume of 500 μl and incubated for 2 hours. Images of germinated pollen grains and the formed pollen tubes were taken with a Nikon Diaphot inverted microscope. The percentage of burst pollen tubes was calculated by the amount of burst pollen tubes from 100 counted pollen grains per treatment. Experiments were repeated more than three times. To further image *Pf*Avr4-2^{RR} on pollen tubes, tomato pollen grains were pregerminated in the pollen germination media buffer amended with 0.5 mM $CaCl_2$ for 2 hours at room temperature. The germinated pollen grains ($n = 1000$) were incubated with 2 μM *Pf*Avr4-2^{RR} in 500 μl of pollen germination media buffer for 40 min at room temperature. The pollen grains were collected via centrifugation at 2000 rpm for 3 min and washed with the pollen germination media buffer three times. Images of at least 10 pollen tubes were taken with a Leica LAS-AF SPE confocal microscope (Leica Camera) at ×40 magnification.

Stable expression of *PfAvr4-2* in tomato plants

To express *PfAvr4-2* in Moneymaker plants, *A. tumefaciens* GV3101 that was transformed with a binary pMOG800 vector in which the mature *PfAvr4-2* was cloned was submitted to the Plant Transformation Facility of the UC Davis (https://ptf.ucdavis.edu/) for generating transgenic plants according to an established protocol used by the facility (Supplementary Materials and Methods). The *PfAvr4-2* transgene expressed in Moneymaker consisted of the mature *PfAvr4-2* protein, fused to the *N. tabacum* PR1A signal sequence for secretion into the apoplast, and placed in-between the cauliflower mosaic virus 35*S* promoter (*CaMV* 35*S*) and the *Agrobacterium* nopaline synthase terminator. The presence of the *PfAvr4-2* transgene in T_1 plants was confirmed by PCR using primers PR1A_ClaI_F/*PfAvr4-2*_NotI_R (table S1). At least five T_1 plants with the *PfAvr-2* transgene were selected and self-fertilized. The derived T_2 lines were germinated on Murashige and Skoog minimal organics (MSO) medium amended with kanamycin sulfate (50 mg/liter), and the presence of the *PfAvr4-2* transgene was reconfirmed by PCR using the above primers. T_2 plants were then self-fertilized, and 11 seeds were tested for segregation by placing them on MSO medium amended with kanamycin sulfate (50 mg/liter). Of the 11 seeds, seven produced seedlings that survived the selection and continued to grow, indicating that they are homozygous for *PfAvr4-2*. Two T_2 lines (35*S*::*PfAvr4-2_1* and 35*S*::*PfAvr4-2_2*) were lastly selected,

and the expression levels of the *PfAvr4-2* transgene in each line were examined by qPCR relative to the tomato *RPL2* gene using the primers *Pf*Avr4-2_qPCR-F/*Pf*Avr4-2_qPCR-R and TmRRL2-F/TmRPL2-R (table S1).

Extraction of pectin from tomato leaves and immunodot blot analysis

Extraction of pectin and of Ca^{2+}-mediated cross-linked homogalacturonan from plant cell walls of the two 35*S::PfAvr4-2* transgenic lines and the control Moneymaker line was performed as described before (*42*), with some modifications. Briefly, 1 g of tomato leaves collected from 6-week-old plants was ground to fine powder in liquid nitrogen, washed with 5 ml of 70% ethanol, incubated at room temperature with rotation for 10 min, and pelleted by centrifugation at 5000 rpm for 10 min. The washing step was repeated five times until all chlorophyll was removed. The pellet was then resuspended in 5 ml of 100% acetone, incubated for 10 min at room temperature with rotation, and centrifuged at 5000 rpm for 10 min. The supernatant was decanted, and the pellet that contained the alcohol-insoluble residue (AIR) was air-dried overnight. Pectin was extracted from 10 mg of AIR by adding 300 µl of 50 µM cyclohexane diamine tetraacetic acid (CDTA; pH 7.0), vortexing the sample at room temperature for 2 hour, and centrifuging at 12,000 rpm for 10 min. The supernatant was then stored at 4°C until immunodot blot analysis. Since CDTA removes Ca^{2+} from pectin, to extract Ca^{2+}–cross-linked homogalacturonan, 10 mg of AIR was mixed with 300 µl of ddH_2O and then vortexed at room temperature for 2 hours. After centrifugation, the supernatant was stored at 4°C.

Immunodot blot analysis was performed as described before (*43*), with some modifications. Briefly, to determine the amount of Ca^{2+}-mediated cross-linking in the above samples, they were diluted 10×, 20×, and 40× in ddH_2O, and 1 µl of each diluted sample was applied to a nitrocellulose membrane (Sigma-Aldrich). The membrane was then dried at 37°C for 1 hour and blocked with 1× phosphate-buffered saline with 3% milk (PBS/M) [137 mM NaCl, 2.7 mM KCl, 10 mM Na_2HPO_4, and 1.8 mM KH_2PO_4 (pH 7.4)] for 1 hour. Next, the 2F4 antibody was diluted 1:250 in PBS/M buffer and incubated with the membrane overnight. The next day, the membrane was washed three times with the PBS buffer and incubated with the goat anti-mouse IgG (H + L) secondary monoclonal antibody conjugated to the horseradish peroxidase (HRP) enzyme (Cell Signaling Technology) in PBS/M buffer in a 1:2500 dilution for 1 hour. The membrane was then washed with PBS buffer three times, and the signal was developed using the TMB substrate Kit (Vector Laboratories), following the manufacturer's protocol. To quantify the amount of pectin extracted with CDTA from the AIR samples, we followed the same procedure but using the JIM5 antibody and anti-rat IgG (H + L) secondary monoclonal antibody conjugated with HRP (Cell Signaling Technology). The fluorescent signal from the 2F4 or JIM5 antibodies was detected using ChemiDoc MP (Bio-Rad). All immunodot blot results were analyzed and quantified using the Image Lab software (v6.0.0 build 26, Bio-Rad). The experiments were repeated five times with reproducible results. Statistical analysis was performed using GraphPad Prism software (v8.3.1, GraphPad software Inc.). One-way analysis of variance (ANOVA) with a Tukey's test ($\alpha = 0.05$) was performed to evaluate the difference between different treatments.

CoMPP and monosaccharide composition analysis

Freeze-dried leaves of the two 35*S::PfAvr4-2* transgenic lines and the control Moneymaker line were homogenized into fine powder, and the material was washed five times for 10 min and two times for 60 min in 70% ethanol under rotation at room temperature. The material was pelleted between washes by centrifugation for 10 min at 4500 rpm, and the supernatant was decanted. The pellet was subsequently washed in $CHCl_3$:CH_3OH 1:1 (v/v) for 2 hours and lastly in 100% acetone for 2 hours. Residual acetone was evaporated overnight in a fume hood, and the resulting cell wall–enriched fractions of AIR were used for CoMPP and monosaccharide composition analysis.

CoMPP was carried out as described before (*27*), with some modifications. Briefly, 10 mg of AIR was sequentially treated with 400 µl of 50 mM CDTA (pH 7.5) to primarily extract pectins and 4 M NaOH with 0.1% (w/v) $NaBH_4$ to primarily extract hemicelluloses. Each extraction was carried out for 2 hours under shaking in a Tissue lyser (QIAGEN) at 7 s^{-1} at room temperature. Samples were pelleted in between extractions by centrifugation at 4500 rpm for 15 min. The extracts were printed on nitrocellulose membrane in two technical replicates and four dilutions using an Arrayjet Marathon (Arrayjet, Roslin, UK). The resulting microarrays were probed with different monoclonal antibodies and quantified as described by Moller *et al.* (*44*). The details on antiglycan antibodies and respective epitopes can be found in Rydahl *et al.* (*45*).

For monosaccharide composition analysis, AIR material was destarched as follows: 40 mg of AIR was transferred to 2-ml tubes, together with two glass beads and 450 µl of preheated (85°C) MOPS buffer [50 mM 4-morpholinepropanesulfonic acid sodium salt, 5 mM $CaCl_2$, and 0.02% NaN_3 (pH 7.0)]. The mixture was heated to 85°C for 5 min to allow for starch gelatinization, and 4 µl of termamyl ultrapure amylase (activity, 179 KNU/g; Novozymes) was added to it and incubated at 85°C for 1.5 hours in a heating block at 500 rpm. The mixture was then cooled to 50°C, and the pH was adjusted to 4.5 with CH_3COOH before adding 1.8 U of amyloglucosidase (A-3042, Sigma-Aldrich) and 0.5 U of isoamylase (E-ISAMY, Megazyme) and incubating at 50°C for 1 hour in a heating block at 500 rpm. Last, ethanol was added to 70% and the sample was allowed to precipitate at 4°C overnight. The following day, the samples were centrifuged at 14,000 rpm for 15 min, washed three times in 70% ethanol, and dried overnight under vacuum. For the analysis, 10 mg of destarched AIR was hydrolyzed in 2 M trifluoroacetic acid (TFA) at 120°C for 1 hour. TFA was removed by drying under vacuum. The hydrolysates were dissolved in ddH_2O, and monosaccharide composition was determined by high HPAEC-PAD using a PA20 column (Dionex) at a flow rate of 0.45 ml/min. Monosaccharide standards were L-Fuc, L-Rha, L-Ara, D-Gal, D-Glc, D-Xyl, D-Man, D-GalUA, and D-GlcA (Sigma-Aldrich). Statistical analysis was performed using RStudio (v4.0.0, RStudio Core Team). One-way ANOVA with a Tukey's test ($\alpha = 0.05$) was performed to evaluate the difference between different lines.

Characterization of the morphological, anatomical, and textural properties of the 35*S::PfAvr4-2*–expressing tomato plants

Transgenic tomato plants were grown as described above. The height of 14 6-week-old plants per line was determined by measuring stem length from the cotyledons till the shoot tip. To determine the size and number of cells in the cortex, 2-week-old seedlings

were cut at 1 cm from the base of the crown and sectioned into 150-µm-thick sections using a Vibratome-1000, as described above. Images of the stem cross sections were taken with a Leica SP8 confocal microscope (Leica Camera) at ×40 magnification, and they were combined and constructed using the navigation tool feature of the Leica LAS X software (v2.0.0.144332). The average cell size in the cortex was determined by calculating the total cortex area in the stem using the drawing tool in the Fiji software (v2.0.0-rc-62/1.51s) and dividing it by the number of cells in the cortex. All experiments were repeated three times with reproducible results.

The texture of petiole tissue from transgenic (35S::*PfAvr4-2_1* and 35S::*PfAvr4-2_2*) and control Moneymaker plants was assessed using an indentation test (*46*). Briefly, petioles were carefully removed with a razor from the main stem, placed on their side on a metal platform, and immobilized with tape. Petioles were then compressed in the direction perpendicular to their long axis using a texture analyzer (TA-XT Plus, Texture Technologies Corp.) equipped with a 1-mm-diameter cylindrical probe. The test was conducted at 0.1 mm/s and was stopped when 33% strain was reached. The test was conducted at room temperature, and data were acquired at 250 Hz. All indentation tests on a given petiole were carried out within 10 min of removal from the plant stem. The parameters that were obtained from texture analysis were maximum force (in newton), defined as the highest normal on the probe achieved during the test, stiffness (in newton per millimeter), defined as the maximum force achieved during the test divided by the total displacement of the probe, and distance at fracture (in millimeter), quantified as the displacement of the probe when the first significant fracture (breakage) of the petiole tissue occurred (*47*). The first significant fracture of the petiole tissue was defined as the first peak in the texture curve (force versus distance) with prominence >0.015 N, which was used to ensure that a consistent criterion was applied to all samples. Parameters obtained from texture analysis are presented using an exemplary texture curve in Fig. 6A. The experiment was repeated three times and at least 29 petioles were tested per line, resulting in a minimum of 115 total compression tests per line. Statistical analysis was performed using GraphPad Prism software (v8.3.1, GraphPad software Inc.). One-way ANOVA with a Tukey's test ($\alpha = 0.05$) was conducted to compare different treatments.

Expression analysis and virulence assays

Inoculation of the Moneymaker tomato line or of the 35S::*PfAvr4-2* transgenic plants with *P. fuligena* wild-type (WT) strain or the two derivative Δ*PAfr4-2* knockout strains (Δ*Pf*Avr4-2_1 and Δ*Pf*Avr4-2_2), analysis of *PfAvr4* and *PfAvr4-2* expression, and quantification of the fungal biomass at 9 days after inoculation were performed as described before (*19*). The *PfAvr4-2* deletion mutants were generated by replacing the *PfAvr4-2* gene with the geneticin resistance cassette as described before (*19*), with some modifications (Supplementary Materials and Methods). For each assayed strain, nine inoculated leaves from three tomato plants were collected at 1, 3, 6, 9, and 12 days after inoculation. Total RNA was extracted using TRIzol (Life Technologies), and complementary DNA (cDNA) was produced using the iScript cDNA Synthesis Kit (Bio-Rad). The biomass of *P. fuligena* during fungal infection was quantified by qPCR using fungal actin and the tomato *RPL2* gene for calibration, with the primers listed in table S1. qPCR was conducted in a CFX96 Touch Real-Time PCR detection system (Bio-Rad) equipped with the CFX Maestro Software. The reaction cycles consisted of an initial 95°C for 10 min, followed by 15 s at 95°C, 30 s at 60°C, and 30 s at 72°C for 40 cycles. The expression of *PfGAPDH* was used as an endogenous control that was set to 1.0 for calculating the relative expression of *PfAvr4-2*. For the virulence assays, the relative biomass of *P. fuligena* during infection was based on the expression of *PfActin* as compared to *TmRPL2* transcripts. Virulence assays and qPCRs were performed in triplicate. Statistical analysis was performed using GraphPad Prism software (v8.3.1, GraphPad software Inc.). One-way ANOVA with a Tukey's test ($\alpha = 0.05$) was conducted to compare different treatments. Expression analysis of *PfAvr4-2* was performed twice.

To inoculate leaves of the 35S::*PfAvr4-2* transgenic plants with *B. cinerea* strain B05.10, detached leaves from 6-week-old tomato plants were placed on 1% water phytoagar (Thomas Scientific) in plastic trays covered with a lid to retain humidity. Conidia of *B. cinerea* were collected from a 2-week-old culture grown on potato dextrose agar and resuspended to 5000 spores/ml in 50% organic grape juice. A single 4-µl droplet of the conidial suspension was then placed on the abaxial side of the tomato leaves. Images of five to six inoculated leaves were taken at 4 days after inoculation, and the diameters (i.e., sizes) of infection lesions from 10 inoculation sites were measured with the Fiji software (*48*). The size of the infection lesions on leaves of the two 35S::*PfAvr4-2* transgenic lines was calculated relative to their size on the control Moneymaker plants, which was set to 1.0. Infection assays with *B. cinerea* were repeated three times with reproducible results. Statistical analysis was performed using GraphPad Prism software (v8.3.1, GraphPad software Inc.). One-way ANOVA with a Tukey's test ($\alpha = 0.05$) was conducted to compare different treatments.

Quantification of PME, PG, and pectate lyase activity

To quantify the enzymatic activity of PMEs, PGs, and pectate lyases, we used an agarose diffusion assay as described before (*29*), with some modifications. Briefly, 100 µg of *Pf*Avr4-2 was mixed with 10 ml of SDS buffer (62.5 mM tris, 715 mM β-mercaptoethanol, and 346.78 mM $NaC_{12}H_{25}SO_4$) and boiled for 10 min. The boiled protein was precipitated with 20% (w/v) trichloroacetic acid overnight at 4°C, pelleted by centrifugation at 14,000 rpm for 30 min at 4°C, and washed with cold 100% acetone. After centrifuging the samples at 14,000 rpm for 20 min at 4°C, the acetone was removed by aspiration, and the pelleted protein was dried at room temperature for 30 min. Last, the protein was resuspended in the NaOAc/NaCl buffer. Fungal PMEs were extracted from the culture media of 4-day-old *B. cinerea* cultures in Gamborg B5 medium in which 0.5% apple pectin (w/v; Sigma-Aldrich) was used as the sole carbon source. The culture filtrates were first passed through a Whatman GFA filter paper (Sigma-Aldrich) and then through a bottle-top vacuum filter with a 0.45-µm polyethersulfone membrane (Olympus Plastics). The total protein was concentrated to a small volume using an Amicon Ultra-15 centrifugal filter unit (3-kDa cutoff, Millipore) and stored at −80°C. *Pf*Avr4-2 was next incubated with a fungal PME, fungal endo-PG (Sigma-Aldrich, catalog no. 17389), exo-PG (Megazyme, catalog no. E-EXPGA), or pectate lyase (Megazyme, catalog no. E-PCLYAN) in wells ($n = 2$ per pectoplate per treatment) of the pectoplates ($n = 3$ per treatment) as follows: The pectoplate was prepared with 0.1% (w/v) apple pectin, 1% agarose, 25 mM NaOAc (pH 5.5), and 50 mM NaCl for measuring PME and pectate lyase activities, whereas instead of apple pectin, 0.1% (w/v) polygalacturonic acid (Sigma-Aldrich, catalog no. 81325) was used for detecting the enzymatic activities of

the endo- and exo-PG. Once the gel is polymerized in 120-mm petri dish (50 ml per plate), the mixture of enzymes and proteins (2 mU of enzyme with 40 μM *Pf*Avr4-2 or boiled *Pf*Avr4-2) was loaded into 4-mm wells cut into the pectoplate with a cork borer and incubated at 30°C for 16 hours. The plates were next stained with 0.05% (w/v) Ruthenium Red (Sigma-Aldrich) for 30 min and washed with water until the fuchsia-colored haloes become noticeable on the gel. The size of the fuchsia-stained haloes (n = 9) was measured using the Fiji software (v2.0.0-rc-62/1.51s). The PECTOPLATE assays were repeated three times, with two replicates for each treatment included in each experiment. Results were reproducible. Statistical analysis was performed using GraphPad Prism software (v8.3.1, GraphPad software Inc.). Student's t test or one-way ANOVA with a Tukey's test (α = 0.05) was conducted to compare different treatments.

To further confirm the impact of *Pf*Avr4-2 on the enzymatic activity of the endo-PGs, we used a spectrophotometric approach to measure the enzymatic degradation of pectin using 2-cyanoacetamide as described before (*49*). Briefly, 0.5 mg of polygalacturonic acid, 5 mU of the fungal endo-PG, and 10 μM of protein samples (*Pf*Avr4, *Pf*Avr4-2, or WGA) were mixed in the NaOAc/NaCl buffer to a final volume of 500 μl at 37°C for 30 min. A total of 1.2 ml of TBC reagent (100 mM $Na_2B_4O_7$, 100 mM H_3BO_3, and 0.1% 2-cyanoacetamide) was added to the reaction mixture and boiled for 10 min to stop the reaction. After cooling, the absorbance of the mixture was determined spectrophotometrically at 276 nm using a SpectraMax Plus 384 microplate reader (Molecular Devices). The experiment was repeated three times with at least three replicates per experiment and reproducible results. Statistical analysis was performed using GraphPad Prism software (v8.3.1, GraphPad software Inc.). Student's t test or one-way ANOVA with a Tukey's test (α = 0.05) was conducted to evaluate the statistical significant differences between treatments.

Recognition of the *Pf*Avr4 and *Pf*Avr4-2 by the tomato Cf-4 receptor.

A. tumefaciens–based transient transformation assays were performed as described before (*19*). The pMOG800 plasmid containing the mature *Pf*Avr4-2 protein was prepared as described above, whereas pMOG800 plasmid containing the mature *Pf*Avr4 or the tomato *Cf-4*–resistant gene was available by the study of Kohler *et al.* (*19*). All plasmids were transformed into *A. tumefaciens* strain GV3101 via electroporation. Transformed agrobacterium with the pMOG800/Cf-4 plasmid was grown to an optical density at 600 nm (OD_{600}) of 0.5, whereas agrobacterium transformed with the pMOG800/*Pf*Avr4 or *Pf*Avr4-2 plasmid was grown to an OD_{600} of 1.0. Each mixture of agrobacterium cultures was infiltrated at least three times, on three leaves of three *N. benthamiana* or *N. tabacum* plants, and infiltrated plants were kept in a growth chamber with 16-hour light and 70% humidity at 25°C for 6 days. The experiment was repeated twice with reproducible results.

Monitoring of ROS burst.

To monitoring ROS-burst following treatment of tomato leaves with an OG10-15 solution, leaf discs of 3.8 mm in diameter from 4- to 5-week-old tomato plants of the two 35*S::PfAvr4-2* transgenic lines and the control Moneymaker line were collected and placed overnight at room temperature in a well (one leaf disk per well) of a white 96-well plate (Corning Inc.) with their abaxial side phasing up and in 200 μl of water. After removing the water from the wells, 100 μl of assay solution containing 1.25 μM chemiluminescent probe L-012 (Wako Chemicals, catalog no. 075-05111), peroxidase (20 μg/ml; Sigma-Aldrich, catalog no. P6782), and 10 μM OG10-15 solution (Carbosynth, catalog no. OG59704) was added to the bottom of each well without damaging and submerging the leaf discs. Mock treatments consisted of the same assay solution without the OG10-15 solution. The production of chemiluminescence from each well was measured immediately using a TriStar LB 941 microplate reader (Berthold Technologies). Experiments were repeated three times with reproducible results and with four leaves monitored per line per assay.

Statistical analysis

Student's t test or one-way ANOVA with a Tukey's test (α = 0.05) was conducted to evaluate the statistical significance among treatments, as described in individual experiments.

SUPPLEMENTARY MATERIALS

Supplementary material for this article is available at http://advances.sciencemag.org/cgi/content/full/7/19/eabe0809/DC1

View/request a protocol for this paper from *Bio-protocol*.

REFERENCES AND NOTES

1. J. D. G. Jones, J. L. Dangl, The plant immune system. *Nature* **444**, 323–329 (2006).
2. L. Bacete, H. Mélida, E. Miedes, A. Molina, Plant cell wall-mediated immunity: Cell wall changes trigger disease resistance responses. *Plant J.* **93**, 614–636 (2018).
3. G. De Lorenzo, S. Ferrari, M. Giovannoni, B. Mattei, F. Cervone, Cell wall traits that influence plant development, immunity, and bioconversion. *Plant J.* **97**, 134–147 (2019).
4. K. H. Caffall, D. Mohnen, The structure, function, and biosynthesis of plant cell wall pectic polysaccharides. *Carbohydr. Res.* **344**, 1879–1900 (2009).
5. F. Sénéchal, C. Wattier, C. Rustérucci, J. Pelloux, Homogalacturonan-modifying enzymes: Structure, expression, and roles in plants. *J. Exp. Bot.* **65**, 5125–5160 (2014).
6. D. E. Ngouémazong, R. P. Jolie, R. Cardinaels, I. Fraeye, A. Van Loey, P. Moldenaers, M. Hendrickx, Stiffness of Ca^{2+}–pectin gels: Combined effects of degree and pattern of methylesterification for various Ca^{2+} concentrations. *Carbohydr. Res.* **348**, 69–76 (2012).
7. S. Wolf, G. Mouille, J. Pelloux, Homogalacturonan methyl-esterification and plant development. *Mol. Plant* **2**, 851–860 (2009).
8. M. S. Zamil, A. Geitmann, The middle lamella-more than a glue. *Phys. Biol.* **14**, 015004 (2017).
9. V. Lionetti, F. Cervone, D. Bellincampi, Methyl esterification of pectin plays a role during plant-pathogen interactions and affects plant resistance to diseases. *J. Plant Physiol.* **169**, 1623–1630 (2012).
10. A. Brutus, F. Sicilia, A. Macone, F. Cervone, G. De Lorenzo, A domain swap approach reveals a role of the plant wall-associated kinase 1 (WAK1) as a receptor of oligogalacturonides. *Proc. Natl. Acad. Sci. U.S.A.* **107**, 9452–9457 (2010).
11. H. W. Choi, D. F. Klessig, DAMPs, MAMPs, and NAMPs in plant innate immunity. *BMC Plant Biol.* **16**, 232 (2016).
12. S. Ferrari, D. V. Savatin, F. Sicilia, G. Gramegna, F. Cervone, G. De Lorenzo, Oligogalacturonides: Plant damage-associated molecular patterns and regulators of growth and development. *Front. Plant Sci.* **4**, 49 (2013).
13. J. C. Cabrera, A. Boland, J. Messiaen, P. Cambier, P. Van Cutsem, Egg box conformation of oligogalacturonides: The time-dependent stabilization of the elicitor-active conformation increases its biological activity. *Glycobiology* **18**, 473–482 (2008).
14. A. Voxeur, O. Habrylo, S. Guénin, F. Miart, M.-C. Soulié, C. Rihouey, C. Pau-Roblot, J.-M. Domon, L. Gutierrez, J. Pelloux, G. Mouille, M. Fagard, H. Höfte, S. Vernhettes, Oligogalacturonide production upon *Arabidopsis thaliana–Botrytis cinerea* interaction. *Proc. Natl. Acad. Sci. U.S.A.* **116**, 19743–19752 (2019).
15. H. Cui, K. Tsuda, J. E. Parker, Effector-triggered immunity: From pathogen perception to robust defense. *Annu. Rev. Plant Biol.* **66**, 487–511 (2015).
16. T. Y. Toruño, I. Stergiopoulos, G. Coaker, Plant-pathogen effectors: Cellular probes interfering with plant defenses in spatial and temporal manners. *Annu. Rev. Phytopathol.* **54**, 419–441 (2016).
17. N. K. Hurlburt, L.-H. Chen, I. Stergiopoulos, A. J. Fisher, Structure of the *Cladosporium fulvum* Avr4 effector in complex with $(GlcNAc)_6$ reveals the ligand-binding mechanism and uncouples its intrinsic function from recognition by the Cf-4 resistance protein. *PLOS Pathog.* **14**, e1007263 (2018).

18. I. Stergiopoulos, H. A. van den Burg, B. Ökmen, H. G. Beenen, S. van Liere, G. H. J. Kema, P. J. G. M. de Wit, Tomato Cf resistance proteins mediate recognition of cognate homologous effectors from fungi pathogenic on dicots and monocots. *Proc. Natl. Acad. Sci. U.S.A.* **107**, 7610–7615 (2010).
19. A. C. Kohler, L.-H. Chen, N. Hurlburt, A. Salvucci, B. Schwessinger, A. J. Fisher, I. Stergiopoulos, Structural analysis of an Avr4 effector ortholog offers insight into chitin binding and recognition by the Cf-4 receptor. *Plant Cell* **28**, 1945–1965 (2016).
20. T.-C. Chang, A. Salvucci, P. W. Crous, I. Stergiopoulos, Comparative genomics of the Sigatoka disease complex on banana suggests a link between parallel evolutionary changes in *Pseudocercospora fijiensis* and *Pseudocercospora eumusae* and increased virulence on the banana host. *PLOS Genet.* **12**, e1005904 (2016).
21. C. Brett, K. Waldron, *Physiology and Biochemistry of Plant Cell Walls* (Unwin Hyman, London, Boston, 1990), Topics in plant physiology, pp. xiv, 194 p.
22. D. Mohnen, Pectin structure and biosynthesis. *Curr. Opin. Plant Biol.* **11**, 266–277 (2008).
23. M. H. Clausen, W. G. T. Willats, J. P. Knox, Synthetic methyl hexagalacturonate hapten inhibitors of anti-homogalacturonan monoclonal antibodies LM7, JIM5 and JIM7. *Carbohydr. Res.* **338**, 1797–1800 (2003).
24. S. T. de Freitas, A. K. Handa, Q. Wu, S. Park, E. J. Mitcham, Role of pectin methylesterases in cellular calcium distribution and blossom-end rot development in tomato fruit. *Plant J.* **71**, 824–835 (2012).
25. J. Mravec, S. K. Kračun, M. G. Rydahl, B. Westereng, D. Pontiggia, G. De Lorenzo, D. S. Domozych, W. G. T. Willats, An oligogalacturonide-derived molecular probe demonstrates the dynamics of calcium-mediated pectin complexation in cell walls of tip-growing structures. *Plant J.* **91**, 534–546 (2017).
26. E. Parre, A. Geitmann, More than a leak sealant. The mechanical properties of callose in pollen tubes. *Plant Physiol.* **137**, 274–286 (2005).
27. S. K. Kračun, J. U. Fangel, M. G. Rydahl, H. L. Pedersen, S. Vidal-Melgosa, W. G. T. Willats, Carbohydrate microarray technology applied to high-throughput mapping of plant cell wall glycans using comprehensive microarray polymer profiling (CoMPP), in *High-Throughput Glycomics and Glycoproteomics* (Springer, 2017), pp. 147–165.
28. I. B. Ferguson, Calcium in plant senescence and fruit ripening. *Plant Cell Environ.* **7**, 477–489 (1984).
29. V. Lionetti, PECTOPLATE: The simultaneous phenotyping of pectin methylesterases, pectinases, and oligogalacturonides in plants during biotic stresses. *Front. Plant Sci.* **6**, 331 (2015).
30. R. de Jonge, H. P. van Esse, A. Kombrink, T. Shinya, Y. Desaki, R. Bours, S. van der Krol, N. Shibuya, M. H. A. J. Joosten, B. P. H. J. Thomma, Conserved fungal LysM effector Ecp6 prevents chitin-triggered immunity in plants. *Science* **329**, 953–955 (2010).
31. A. B. Boraston, D. N. Bolam, H. J. Gilbert, G. J. Davies, Carbohydrate-binding modules: Fine-tuning polysaccharide recognition. *Biochem. J.* **382**, 769–781 (2004).
32. V. Reyes-Ortiz, R. A. Heins, G. Cheng, E. Y. Kim, B. C. Vernon, R. B. Elandt, P. D. Adams, K. L. Sale, M. Z. Hadi, B. A. Simmons, M. S. Kent, D. Tullman-Ercek, Addition of a carbohydrate-binding module enhances cellulase penetration into cellulose substrates. *Biotechnol. Biofuels* **6**, 93 (2013).
33. L. Sella, C. Castiglioni, M. C. Paccanaro, M. Janni, W. Schäfer, R. D'Ovidio, F. Favaron, Involvement of fungal pectin methylesterase activity in the interaction between *Fusarium graminearum* and wheat. *Mol. Plant Microbe Interact.* **29**, 258–267 (2016).
34. O. Valette-Collet, A. Cimerman, P. Reignault, C. Levis, M. Boccara, Disruption of *Botrytis cinerea* pectin methylesterase gene Bcpme1 reduces virulence on several host plants. *Mol. Plant Microbe Interact.* **16**, 360–367 (2003).
35. D. J. Cosgrove, Growth of the plant cell wall. *Nat. Rev. Mol. Cell Biol.* **6**, 850–861 (2005).
36. D. J. Cosgrove, Plant expansins: Diversity and interactions with plant cell walls. *Curr. Opin. Plant Biol.* **25**, 162–172 (2015).
37. S. Wawra, P. Fesel, H. Widmer, M. Timm, J. Seibel, L. Leson, L. Kesseler, R. Nostadt, M. Hilbert, G. Langen, A. Zuccaro, The fungal-specific β-glucan-binding lectin FGB1 alters cell-wall composition and suppresses glucan-triggered immunity in plants. *Nat. Commun.* **7**, 13188 (2016).
38. K. Tamura, G. Stecher, D. Peterson, A. Filipski, S. Kumar, MEGA6: Molecular evolutionary genetics analysis version 6.0. *Mol. Biol. Evol.* **30**, 2725–2729 (2013).
39. J. Yang, R. Yan, A. Roy, D. Xu, J. Poisson, Y. Zhang, The I-TASSER Suite: Protein structure and function prediction. *Nat. Methods* **12**, 7–8 (2015).
40. E. F. Pettersen, T. D. Goddard, C. C. Huang, G. S. Couch, D. M. Greenblatt, E. C. Meng, T. E. Ferrin, UCSF Chimera—A visualization system for exploratory research and analysis. *J. Comput. Chem.* **25**, 1605–1612 (2004).
41. P. A. Covey, C. C. Subbaiah, R. L. Parsons, G. Pearce, F. T. Lay, M. A. Anderson, C. A. Ryan, P. A. Bedinger, A pollen-specific RALF from tomato that regulates pollen tube elongation. *Plant Physiol.* **153**, 703–715 (2010).
42. I. E. Moller, F. A. Pettolino, C. Hart, E. R. Lampugnani, W. G. T. Willats, A. Bacic, Glycan profiling of plant cell wall polymers using microarrays. *J. Vis. Exp.*, e4238 (2012).
43. C. Hervé, S. E. Marcus, J. P. Knox, Monoclonal antibodies, carbohydrate-binding modules, and the detection of polysaccharides in plant cell walls, in *The Plant Cell Wall* (Springer, 2011), pp. 103–113.
44. I. Moller, I. Sørensen, A. J. Bernal, C. Blaukopf, K. Lee, J. Øbro, F. Pettolino, A. Roberts, J. D. Mikkelsen, J. P. Knox, A. Bacic, W. G. T. Willats, High-throughput mapping of cell-wall polymers within and between plants using novel microarrays. *Plant J.* **50**, 1118–1128 (2007).
45. M. G. Rydahl, A. R. Hansen, S. K. Kračun, J. Mravec, Report on the current inventory of the toolbox for plant cell wall analysis: Proteinaceous and small molecular probes. *Front. Plant Sci.* **9**, 581 (2018).
46. S. Uluisik, N. H. Chapman, R. Smith, M. Poole, G. Adams, R. B. Gillis, T. M. D. Besong, J. Sheldon, S. M. Stiegelmeyer, L. Pérez, N. Samsulrizal, D. Wang, I. D. Fisk, N. Yang, C. Baxter, D. Rickett, R. Fray, B. Blanco-Ulate, A. Powell, S. Harding, J. Craigon, J. Rose, E. A. Fich, L. Sun, D. Domozych, P. Fraser, G. Tucker, D. Grierson, G. Seymour, Genetic improvement of tomato by targeted control of fruit softening. *Nat. Biotechnol.* **34**, 950–952 (2016).
47. C. Skamniotis, M. Elliott, M. Charalambides, Computer simulations of food oral processing to engineer teeth cleaning. *Nat. Commun.* **10**, 3571 (2019).
48. J. Schindelin, I. Arganda-Carreras, E. Frise, V. Kaynig, M. Longair, T. Pietzsch, S. Preibisch, C. Rueden, S. Saalfeld, B. Schmid, J.-Y. Tinevez, D. J. White, V. Hartenstein, K. Eliceiri, P. Tomancak, A. Cardona, Fiji: An open-source platform for biological-image analysis. *Nat. Methods* **9**, 676–682 (2012).
49. S. Honda, Y. Nishimura, M. Takahashi, H. Chiba, K. Kakehi, A manual method for the spectrophotometric determination of reducing carbohydrates with 2-cyanoacetamide. *Anal. Biochem.* **119**, 194–199 (1982).

Acknowledgments: We are thankful to A. Kohler and A. Salvucci for the assistance during the initial phases of this work. We thank M. G. Rydahl for the assistance with the carbohydrate microarrays. We are grateful to B. Mattei and G. de Lorenzo for the critical comments and assisting with some of the early assays. We are thankful to G. Bornhorst and C. Swackhamer for the critical contributions to equipment and for assistance with the texture analyzer experiments. We thank E. Mitcham for providing the PME-silenced tomato lines and C. Nakashima for providing the strains of *P. fuligena*. L. Epstein and R. Bostock are acknowledged for the critical discussions. This paper is dedicated to the memory of J.L. who passed away on 24 September 2019 while this manuscript was in preparation. **Funding:** I.S. was partially supported by the USDA-NIFA Hatch project CA-D-PPA-2185-H. S.K.K., J.M., and B.J. were funded by the Villum Foundation projects PLANET (00009283). This work was partially supported by the Research Investments in Science and Engineering (RISE) program of the UC Davis (Award RI-091). **Author contributions:** Conceptualization: L.-H.C., S.K.K., J.M., and I.S.. Primary data collection and analysis: L.-H.C. Secondary data collection and analysis: L.-H.C., S.K.K., K.S.N., and J.M. Funding acquisition: I.S. and B.J. Methodology: L.-H.C., S.K.K., J.M., J.L., B.J., and I.S. Materials: S.K.K., J.M., and B.J. Project administration: I.S. Writing (original draft): L.-H.C. and I.S. Writing (review and editing): L.-H.C., S.K.K., K.S.N., J.M., B.J., J.L., and I.S. **Competing interests:** The authors declare that they have no competing interests. **Data and materials availability:** All data needed to evaluate the conclusions in the paper are present in the paper and/or the Supplementary Materials. Additional data related to this paper may be requested from the authors.

Submitted 29 July 2020
Accepted 18 March 2021
Published 7 May 2021
10.1126/sciadv.abe0809

Citation: L.-H. Chen, S. K. Kračun, K. S. Nissen, J. Mravec, B. Jørgensen, J. Labavitch, I. Stergiopoulos, A diverse member of the fungal Avr4 effector family interacts with de-esterified pectin in plant cell walls to disrupt their integrity. *Sci. Adv.* **7**, eabe0809 (2021).